Energy Economics 143 (2025) 108225

Contents lists available at ScienceDirect

Energy Economics

journal homepage: www.elsevier.com/locate/eneeco

Modelling time-varying volatility spillovers across crises: Evidence from major commodity futures and the US stock market

Shietal Ramesh [a,*], Rand Kwong Yew Low [a,b], Robert Faff [c,b,a]

[a] Bond Business School, Bond University, Robina, 4226, Australia
[b] UQ Business School, The University of Queensland, Brisbane, 4072, Australia
[c] Corvinus University of Budapest, Budapest, 1093, Hungary

ARTICLE INFO

JEL classification:
G1
C5
C6
C8

Keywords:
Volatility spillover index
Bayesian sampling technique
Crisis period
Risk diversification

ABSTRACT

Effective risk management requires discernment of volatility interaction patterns across assets. Our study examines the level of interconnectedness amongst nine major commodity futures across precious metals, energy, industrial and agricultural sectors and the US S&P 500 index from 1990 to 2022. Spillover indices are constructed by combining the Time-Varying Parameter (TVP)-Vector Autoregression (VAR)-Stochastic Volatility (SV) model with the DY- spillover index. We analyse the fluctuating dynamics of the extent and directionality of the volatility transmissions across various crises. Our results indicate that SPX is the largest net transmitter of volatility information, predominantly affecting crude oil, heating oil, and gold futures, with spillovers intensifying during crises. Gold futures receive heightened volatility transmissions during crises, alluding to the "flight to quality" characteristic displayed by investors. The COVID-19 crisis and the consequent supply chain disruptions uniquely heightened volatility transmissions from lumber to natural gas futures, unseen in previous economic crises. We posit that natural gas futures could be a viable asset for risk diversification as they show limited interaction with SPX and minimal within-sector transmissions with crude and heating oil futures. We substantiate our findings on potential hedge assets by constructing dynamic portfolio weights based on minimising pairwise volatility interactions between assets in the portfolio.

1. Introduction

Historically, investors sought commodity futures to hedge against inflation and optimise portfolio strategies. The prices of commodity futures positively correlate with inflation, making them a hedge against unexpected inflation fluctuations (Gorton and Rouwenhorst, 2006; Spierdijk and Umar, 2010; Liu et al., 2023). Commodity futures also negatively correlate with equity and bond returns, making them valuable tools for strategic asset allocation (Erb and Harvey, 2006; Miffre and Rallis, 2007). The *"flight to quality"* by speculators to precious metal futures, especially during crises, has given them the distinction of being *safe-haven assets* (Baur and McDermott, 2010; Lucey and Li, 2014; Baur and Kuck, 2020). Consequently, trading volumes in commodity futures have increased significantly in recent years.[1]

The rise in speculative investment in commodity futures (a feature referred to as financialisation) has facilitated price discovery and risk-sharing among market participants. However, it has also led individual commodity futures' prices to depend on factors beyond supply–demand dynamics. As more investors hold commodity futures and conventional securities concurrently, the risk of exposure to common volatility factors increases (i.e., bad news in one market has a contagion effect on the other and vice versa). Crisis periods further exacerbate the degree of inter-connectedness between various asset markets (Bekaert and Harvey, 2003; Xiao et al., 2019; Joo et al., 2020). Identifying these dynamic linkages contains significant information that will aid in price discovery and improve forecast accuracy (Zhong et al., 2004; Sehgal et al., 2013).

Assessing systemic risk transmissions across asset classes is a critical research area. Successive economic, financial and geo-political crises meant that there is now a greater interest in disentangling the magnitude and nature of cross-asset volatility spillover effects (Caporale et al., 2006; Akca and Ozturk, 2015; Syriopoulos et al., 2015; Ahmed and Huo, 2021; Serra, 2011; Cabrera and Schulz, 2016). Several studies

* Corresponding author.
E-mail addresses: shietal.ramesh@student.bond.edu.au (S. Ramesh), rlow@bond.edu.au (R.K.Y. Low), rfaff@bond.edu.au (R. Faff).

[1] The average annual trading volume for the U.S. commodity futures markets from 1990–1999, 2000–2009, and 2010–2019 was 2.1, 7.6, and 14.1 trillion dollars, respectively. In 2021, the annual trading volume on U.S. commodity futures markets reached an all-time high of 40.6 trillion dollars, which was equivalent to about half of the overall trading volume of the U.S. stock market (Kang et al., 2023).

https://doi.org/10.1016/j.eneco.2025.108225
Received 8 April 2024; Received in revised form 22 October 2024; Accepted 16 January 2025
Available online 1 February 2025

focus on analysing volatility interactions of commodity futures both within Lin and Tamvakis (2001), Gong et al. (2021) and across sectors (Chen et al., 2023; Yıldırım et al., 2020; Kang et al., 2017; Liu et al., 2021). Studies also investigate integrations between mixed portfolios comprising commodity futures and stock markets (Jebabli et al., 2022; Sarwar et al., 2020; Smales, 2021; Batten et al., 2019).

Current research on volatility spillovers is subject to several limitations. First, most studies focus on two or three sectors and are usually restricted to timelines of under a decade due to computational constraints. Broadening the scope to include a wider range of sectors over a longer timeframe would yield more comprehensive insights into the extent and directionality of spillovers, particularly in capturing transmission patterns during periods of heightened uncertainty. Second, there is limited research analysing differences in volatility spillover behaviours among futures belonging to a similar category,such as the spillover trends between gold and silver futures and between energy futures like crude oil and natural gas futures. Third, there is limited research analysing differences in volatility transmissions depending on the nature of the crises. An economic crisis like the GFC is characterised by illiquidity and a general lack of confidence in the stock market (Xu et al., 2018). Stock markets transmit the increase in volatility to energy futures due to exposure to common shocks. The uncertainty also increases the volatility of precious metal futures as investors seek more stable hedge assets. Alternatively, the COVID-19 pandemic-induced crisis and the consequent lockdowns triggered unprecedented volatility trends in futures unobserved during earlier crises. Lumber futures, for example, experienced record levels of price increases unseen during previous crises.[2] Meanwhile, oil futures experienced historic lows, with WTI crude oil futures even reaching negative levels for the first time in recorded history.[3] These unique volatility situations could potentially translate to unique spillovers currently under-explored in the literature.

Motivated by these aforementioned limitations, our study adopts the TVP-VAR model with SV (Primiceri, 2005; Nakajima, 2011) to capture the dynamic volatility interactions across major commodity futures and SPX. The model uses Bayesian Markov Chain Monte Carlo (MCMC) sampling techniques to estimate the posterior estimates of the time-varying parameters. To construct the dynamic volatility spillover indices, we incorporate the generalised Forecast Error Variance Decomposition (FEVD)-based DY-spillover index (Diebold and Yilmaz, 2008, 2012; Diebold and Yılmaz, 2014). The TVP-VAR-SV model effectively captures underlying patterns by accommodating both the directionality and time-varying nature of spillovers, unlike typical multivariate GARCH models (Maghyereh et al., 2016; Gozgor et al., 2016; Khalfaoui et al., 2019; Filis et al., 2011). Additionally, the time-varying posterior estimates of the model eliminate the need for rolling windows and offer greater robustness to outliers compared to DY-spillover estimates derived from standard VAR models (Balcilar et al., 2019; Liow, 2015). The use of time-varying VAR models combined with the DY-connectedness measure to estimate volatility spillovers has been gaining increasing traction in recent research (Korobilis and Yilmaz, 2018; Gong et al., 2021, 2022a,b; Liu et al., 2021; Yıldırım et al., 2020; Bouri et al., 2021b; Sun et al., 2023).

Our contributions are three-fold. First, our study aims to provide a comprehensive analysis of dynamic volatility spillover effects among nine major commodity futures, spanning precious metals, energy, industrial, and agricultural sectors over a 32-year period from January 1990 to February 2022. The basis for selecting the futures includes market capitalisation, academic relevance, safe-haven abilities, and their potential for intra-sector and inter-crisis analysis. To account for the effects of financialisation on futures, we include the S&P 500 index in our analysis.[4] Second, our timeline covers multiple high-volatility periods, including the AFC, the DBC, the GFC, the ESDC, the oil price crash and the COVID-19 pandemic-induced crisis; we aim to provide a nuanced understanding of how these events shape volatility transmission across major commodity futures markets and SPX whilst also analysing differences in transmissions patterns across crises. Third, we identify hedge-asset potential for non-conventional assets based on analysing inter-asset volatility interactions. Fourth, we construct dynamic weighted portfolios with the objective to minimise volatility interactions amongst them and check their profitability levels in comparison with traditional portfolio construction strategies (minimum variance and equally weighted). Our findings are crucial for investors in assessing the added sensitivity of their portfolios to external factors and using this insight to predict future asset volatility more accurately. Policymakers can also better gauge the impacts of heightened overall asset volatility trends due to exacerbated inter-asset volatility interactions, particularly during crises.

Overall, SPX remains the most dominant transmitter of volatility information, actively transmitting to energy and gold futures, exacerbating during crises. The increased contagion risks from SPX to energy futures allude to the financialisation aspect of these futures. Volatility shocks in the SPX market automatically translate to volatility shocks in crude and heating oil futures. In contrast, natural gas futures and SPX do not significantly influence each other. Natural gas futures also do not interact significantly with crude and heating oil futures consistent with literature that their prices have partially decoupled from other energy futures (Mensi et al., 2021c; Erdős, 2012; Ramberg and Parsons, 2012; Gong et al., 2021). Gold futures receive increased volatility information from SPX and energy futures during crises, which is consistent with being safe-haven assets. However, we note a reduction in the magnitude of spillovers received during the COVID crisis compared to earlier crises. The pandemic-induced crisis was by far the most pervasive in inducing heightened volatility transmissions across all sectors, including record volatility transmissions from lumber to natural gas futures unobserved during previous crises. Additionally, we test the profitability of our findings over time by adopting the MVP strategy (Broadstock et al., 2020) to construct portfolios minimising the risk of cross-asset volatility interactions.

The novelty of our research lies in the non-trivial extension of existing studies which allows investors and policymakers to discern differences in the volatility spillover trends over multiple crises, and allowing for identification of potential alternative hedge assets across a range of sectors. Previous research using the TVP-VAR-SV framework has generally focused on smaller systems (i.e., 3–5 variables over less than a decade) due to computational challenges associated with parameter proliferation. To the best of our knowledge, this is the largest TVP-VAR-SV exercise conducted to date (10 asset classes across a 32 year period). We developed a scalable, cluster-optimised Python codebase capable of expanding across any number of variables. Additionally, we provide a more nuanced understanding of the TVP-VAR-SV algorithm by disentangling the impacts of the time-varying contemporaneous and lag propagation terms along with the effects of exogenous shocks into visualisations matching their corresponding matrix computations.

2. Literature review

Volatility spillovers refer to the impacts, both simultaneous and lagged, that volatility in one market has on the volatility of other markets (Chang et al., 2010). The literature on spillover analyses initially

[2] Lumber futures traded at around $407 at the start of 2020 and hit a record high of $1670.50 in May 2021.

[3] On April 20, 2020, WTI crude oil futures saw the most significant drop in its history when prices dropped by 306% and settled at −37.63$ a barrel.

[4] To the best of our knowledge, this is the largest TVP-VAR-SV exercise conducted to date. Data and associated custom cluster-optimised Python code will be available upon request. We ran the algorithm on the ARDC Nectar cluster on a 32-core node with 64 GB RAM. The run-time was approximately 15 h.

centred on examining the degree of regionalisation (fragmentation), in global oil markets. While Adelman (1984) believed that global oil markets operate as a unified entity, subsequent studies by Weiner (1991) and Gülen (1997) used correlation and regression analyses to demonstrate that the markets were, in fact, fragmented, and even exhibited co-movement behaviour.

The increasing popularity of commodity futures, owing to their role as an inflation hedge and safe-haven asset, has reinforced their appeal to investors. This financialisation has significantly transformed how commodity futures interact with other assets (Yang et al., 2021; Basak and Pavlova, 2016; Mensi et al., 2021d). Consequently numerous studies have dissected volatility transmissions between commodity futures both within and across sectors along with analysing the commodity futures-stock market nexus. Lin and Tamvakis (2001) examine the extent of spillovers between New York Mercantile Exchange (NYMEX) and International Petroleum Exchange (IPE) crude oil futures during both overlapping and non-overlapping trading hours. Their findings reveal significant spillovers during overlapping trading hours, as well as next-day lagged effects on the morning prices of IPE. Gong et al. (2021) analyse time-varying directional spillovers among crude oil, heating oil, and natural gas futures, concluding that volatility transmission peaks during crises, such as the GFC and the oil price crash. Additionally, studies investigating volatility interactions between energy futures and precious metal futures also note the presence of heightened volatility interactions from energy futures to precious metals futures during crises (Kang et al., 2017; Mensi et al., 2020, 2023). These intensified transmission effects raise concerns about the effectiveness of precious metal futures as hedging instruments (Yıldırım et al., 2020). Corbet et al. (2021) analyse shifts in the direction of volatility transmissions between WTI oil prices and US stock market during various oil supply shocks. They find that during the 2014–2016 oil price crash, WTI primarily acted as a net receiver of volatility from the U.S. stock and currency markets. However, this dynamic shifted at the onset of the pandemic-induced crisis, with WTI becoming a net-transmitter of volatility as oil prices turned negative. The pandemic-induced crisis led to production shutdowns that affected industrial and agricultural futures in unprecedented ways compared to previous financial or technological crises. Kamal et al. (2021) noted the increase in dependence in agricultural futures early on during the pandemic unlike the GFC. Studies also document heightened volatility interactions during the pandemic between agricultural and energy futures (Tiwari et al., 2022; Hung, 2021), between industrial and precious metal markets (Liu et al., 2021) and between energy and financial markets (Szafranek et al., 2024). Gong et al. (2022a) provided substantial evidence of significant pure contagion effects pervasive across energy, precious metals and agricultural markets observed during the GFC and the pandemic-induced crisis not observed during non-crisis periods. Our research complements existing literature (Mensi et al., 2021d; Kang and Yoon, 2019; Mensi et al., 2023; Bouri et al., 2021b) to provide a comprehensive dynamic overview of volatility transmissions amongst major commodity futures across precious metals, energy, industrial and agricultural futures and the US Stock market index to discern differences in transmissions across crises and test diversification potential of assets in the overall portfolio.

From a methodological perspective, several studies employ variants of the hybrid Multivariate Generalized Autoregressive Conditional Heteroskedasticity (MGARCH) models to quantify the inter-connectedness amongst different asset classes (Mensi et al., 2018; Mandacı et al., 2020; Benlagha et al., 2022). These studies are limited to either capturing the directionality (Gozgor et al., 2016) of the volatility spillover or its time-varying aspect (Filis et al., 2011; Khalfaoui et al., 2019) but not both. Studies also employ constant VAR models with rolling windows to estimate the dynamic interrelations of the variables in the model system (Zhang and Broadstock, 2020; Lovcha and Perez-Laborda, 2020). However, the results from this approach are dependent on window size and are susceptible to the presence of outliers (Liu and Gong, 2020). The estimated constant VAR model might not necessarily capture the underlying heteroskedasticity, nor can the pre-specified lag model always maintain the necessary stationarity conditions.

Enforcing a pre-defined model may not provide the flexibility to capture exceptional circumstances accurately. Allowing a model to have time-varying coefficients gives it enough flexibility (by enabling a data-generating process) to capture its underlying characteristics. This is the essence of the TVP-VAR with SV (developed by Cogley and Sargent, 2005 and Primiceri, 2005). The time-varying VAR model captures the dynamic interrelationships amongst multiple variables, allowing for the analysis of their mutual dependencies and the transmission of shocks across the system. Adding a stochastic volatility (SV) component (introduced by Black, 1976) to the TVP-VAR approach allows the model to account for the changing volatility conditions caused by exogenous shocks. The TVP-VAR-SV model is thus better equipped to capture the shifts in inter-relationships among variables and evolving volatility patterns. Studies have documented the superiority of time-varying parameter models with SV over their constant parameter counterparts (Nakajima, 2011; Chan and Eisenstat, 2018). Constructing time-varying VARs and estimating volatility spillover measures using connectedness measures is increasingly gaining traction (Gong et al., 2021, 2022a; Liu and Gong, 2020; Liu et al., 2021; Yıldırım et al., 2020; Bouri et al., 2021b; Sun et al., 2023; Gong and Xu, 2022; Gong et al., 2022b). The inherent nature of lagged VAR models accommodates the lagged effects of the volatility spillovers. Most empirical work is, however, limited to implementing smaller systems due to complexities in giant parameter estimations and their associated computational difficulties (4–5 asset classes over 10–15 years). These challenges are further intensified when we allow for flexible co-variances in error structures (stochastic volatility)

Our study adopts the TVP-VAR with SV approach to capture the dynamic interrelationships across multiple asset classes. We follow Primiceri (2005) and Nakajima (2011) and use Bayesian MCMC sampling techniques to estimate the posterior estimates of the time-varying parameters. To construct the volatility spillover index, we incorporate the generalised time-varying forecast error variance decompositions estimated from the TVP-VAR-SV model to construct the DY- connectedness index (Diebold and Yilmaz, 2008, 2012; Diebold and Yılmaz, 2014).[5] We also calculate the average volatility spillover contribution from/to asset class i to/from the remaining asset classes j over various crises to investigate the inter-crisis variations in volatility transmissions. Finally, we test the implications of constructing portfolios based on minimising volatility interactions amongst them and test their profitability over time.

3. Method

Assessing interconnectedness across asset classes is crucial for evaluating market stability and contagion risk. A typical measure of interconnectedness is the transfer of Realised Volatility (RV) between asset classes (Baele, 2005; Diebold and Yilmaz, 2008; Bhar and Nikolova, 2009; Malik and Hammoudeh, 2007). RV is defined as the squared root of the sum of weekly squared returns (Andersen and Bollerslev, 1998; Andersen et al., 2003):

$$RV_t = \sqrt{\frac{\sum_{i=1}^{M} r_{t,i}^2}{M}} \tag{1}$$

[5] The initial version of the DY-connectedness index developed by Diebold and Yilmaz (2008) was based on decomposing the forecast error variances using the Cholesky technique to quantify contributions from specific exogenous shocks. However, the decompositions relied on the ordering of variables in the VAR (Heiden, 2015). The connectedness measure only accounted for aggregate spillovers (i.e., from/to each market i, to/from all other markets, added across i) (Diebold and Yilmaz, 2012). To overcome these limitations, Diebold and Yilmaz (2012) use a generalised VAR framework invariant to variable ordering to calculate the directional and net spillover indices across various sectors.

where RV_t is the weekly realised volatility, $r_{t,i}$ is the return of weekday i calculated as $\ln P_t - \ln P_{t-1}$ (where $P_{t,i}$ is the closing price of weekday i) and M represents the number of trading days in week t. To accommodate for the possibility of varying number of trading days in any given week, we normalise the RV value by dividing the number of trading days in that particular week. Finally, we annualise RV_t by: $100\times\sqrt{52 RV_t}$. RV effectively measures the variance in the prices, a high value implies instability in that asset class. To measure the spillover effect of instability to other asset classes, we use the TVP-VAR-SV framework to model the underlying time series. We use the resulting posterior means to calculate the spillover indices between asset classes.

3.1. Model framework

The TVP-VAR-SV framework, developed by Primiceri (2005), incorporates time-varying components into the coefficients and the variance–covariance matrix of the additive innovations. This approach allows the model to capture the underlying non-linearities in the time series whist maintaining the flexibility of a standard VAR model. The parameters follow a random walk specification to approximate the underlying data-generating process (Cogley and Sargent, 2005). The SV component captures the effects of heteroskedastic external shocks on the simultaneous relationships among model variables (Kim et al., 1998). This model thus differentiates between the impacts of external shocks and changes in the propagation mechanism (Primiceri, 2005; Negro and Primiceri, 2015; Lubik and Matthes, 2016).

For our study, y_t will represent weekly RV. The basic Structural Vector Autoregression (SVAR) model is given by:

$$\mathbf{A}_t y_t = C_t + \sum_{m=1}^{k} (\mathbf{P}_{m,t} y_{t-m}) + u_t, \qquad t = 1, \dots, TL \tag{2}$$

where $[y_t]_{n\times 1}$ is the vector of the observed variable, $[C_t]_{n\times 1}$ is a scalar offset, $[\mathbf{A}_t]_{n\times n}$ captures the contemporaneous impact, and $[\mathbf{P}_{m,t}]_{n\times n}$ captures the impact of the previous data points (k lags). The unobserved error term u_t follows $N(0, \boldsymbol{\Sigma}_t'\boldsymbol{\Sigma}_t)$ where $[\boldsymbol{\Sigma}_t]_{n\times n}$ is a diagonal matrix of time-varying standard deviations. We rearrange the equation to be: $y_t = c_t + \sum_{m=1}^{k}(\mathbf{B}_{m,t} y_{t-m}) + \mathbf{A}_t^{-1}\boldsymbol{\Sigma}_t\varepsilon_t, \quad t = 1, \dots, T$ where $[c_t]_{n\times 1} = \mathbf{A}_t^{-1} C_t$ and $[\mathbf{B}_{m,t}]_{n\times n} = \mathbf{A}_t^{-1}\mathbf{P}_{m,t}$. Finally, $\mathbf{A}_t^{-1}u_t = \mathbf{A}_t^{-1}\boldsymbol{\Sigma}_t\varepsilon_t$, where $[\varepsilon_t]_{n\times 1}\sim N(0, \mathbf{I}_n)$.[6] Packing the vectors y_{t-m} horizontally into a single row we define a new variable $[X_t']_{n\times n(kn+1)}$ which is given by:

$$\begin{aligned} X_t' &= \mathbf{I}_n \otimes [1, y_{t-1}', \dots, y_{t-k}'] \\ &= \begin{pmatrix} 1 & y_{t-1}' & \dots & y_{t-k}' & 0 & 0 & \dots & 0 & \dots \\ 0 & 0 & \dots & 0 & 1 & y_{t-1}' & \dots & y_{t-k}' & \dots \\ & & \vdots & & & & & & \ddots \end{pmatrix}. \end{aligned} \tag{3}$$

That is, X_t' just arranges the $kn+1$ entries along the block diagonal. Additionally, define $[\beta_t]_{n(kn+1)\times 1}$, which is packed as:

$$\begin{aligned} \beta_t' = ((c_t)_1, (\mathbf{B}_{1,t})_{1*}, \dots (\mathbf{B}_{k,t})_{1*}, (c_t)_2, (\mathbf{B}_{1,t})_{2*}, \dots (\mathbf{B}_{k,t})_{2*}, \dots, \\ \dots, (c_t)_n, (\mathbf{B}_{1,t})_{n*}, \dots (\mathbf{B}_{k,t})_{n*}), \end{aligned} \tag{4}$$

where $(\mathbf{B}_{p,t})_{q*}$ denotes row q of $\mathbf{B}_{p,t}$. Thus, the model equation can be written as:

$$y_t = X_t'\beta_t + \xi_t, \qquad t = 1, \dots, T \tag{5}$$

where $[\xi_t]_{n\times 1} = \mathbf{A}_t^{-1}\boldsymbol{\Sigma}_t\varepsilon_t$. So in summary note the following:

- X_t can be constructed from the observed data y_t.
- β_t is the time-varying coefficient on all the lagged vectors. β_t has $mn^2 + n$ values per time step.
- Without loss of generality, $\mathbf{A}_t$ can be represented as a lower triangular matrix with its diagonals being ones. General contemporaneous interactions can still exist under this constraint. Intuitively, the lower triangular matrix captures the co-variation amongst the external shocks affecting the model system. Thus, there are $n(n-1)/2$ values to be estimated per time step.

$$\mathbf{A}_t = \begin{bmatrix} 1 & 0 & \dots & 0 \\ \alpha_{21,t} & 1 & \ddots & \vdots \\ \vdots & \ddots & \ddots & 0 \\ \alpha_{n1,t} & \dots & \alpha_{nn-1,t} & 1 \end{bmatrix} \tag{6}$$

- $\boldsymbol{\Sigma}_t$ is a $n \times n$ diagonal matrix representing the impact of the n exogenous shocks per time step: $\boldsymbol{\Sigma}_t = \text{diag}(\sigma_{1,t}, \sigma_{2,t}, \dots, \sigma_{n,t})$.
- The noise term $\xi_t \equiv \mathbf{R}_t\varepsilon_t = \mathbf{A}_t^{-1}\boldsymbol{\Sigma}_t\varepsilon_t$ has $n(n+1)/2$ unique values per time step. The variance–covariance matrix of $\mathbf{R}_t$ is given by:

$$\mathbf{R}_t = \mathbf{A}_t^{-1}\boldsymbol{\Sigma}_t(\mathbf{A}_t^{-1}\boldsymbol{\Sigma}_t)' \tag{7}$$

We take the coefficients in Eq. (5) to follow a first-order random-walk process, i.e, $\beta_t = \beta_{t-1} + \mathcal{V}_t$, $\alpha_t = \alpha_{t-1} + \zeta_t$ and $\log\sigma_{m,t} = \log\sigma_{m,t-1} + \eta_t$. The innovations of the random walk processes are assumed to be jointly normally distributed with the block-diagonal covariance matrix represented as: $\mathbf{V} = Var(\text{diag}[\varepsilon_t', \mathcal{V}_t', \zeta_t', \eta_t'])' = \text{diag}(\mathbf{I}_n, \mathbf{Q}, \mathbf{S}, \mathbf{W})$. Estimation of the TVP-VAR-SV model is computationally intensive due to the high dimensionality of the matrices involved. We adopt Bayesian MCMC algorithms, as developed by Primiceri (2005) and Nakajima (2011), to estimate the posterior values of the parameters and variances, given the model's non-linear and time-varying nature.[7]

3.1.1. Calculating the forecast error variance decomposition-based spillover indices

Diebold and Yilmaz define volatility spillovers as fractions of the H-step ahead forecast error variance in y_i due to a shock in y_j (Diebold and Yilmaz, 2008, 2012; Diebold and Yılmaz, 2014). In order to estimate the spillover index, we first compute the Impulse Response Function (IRF). Writing the VAR(k) model in its associated VAR(1) form, we get:

$$Y_t = \upsilon_t + F_t Y_{t-1} + \mathbf{e}_t \tag{8}$$

where $[Y_t]_{kn\times 1} = [y_t', y_{t-1}', \dots, y_{t-k+1}']'$ is the vector of lagged y_t, $[\upsilon_t]_{kn\times 1} = [c_t', c_{t-1}', \dots, c_{t-k+1}']'$, $[F_t]_{kn\times kn}$ is the transition matrix and $[\mathbf{e}_t]_{kn\times 1}$ is the noise vector:

$$F_t = \begin{pmatrix} \mathbf{B}_{1,t} & \mathbf{B}_{2,t} & \dots & \mathbf{B}_{k,t} \\ \mathbf{I}_{n(k-1)} & & & [\mathbf{0}]_{n(k-1)\times n} \end{pmatrix} \tag{9}$$

$$\mathbf{e}_t = \begin{pmatrix} \mathbf{A}^{-1}\boldsymbol{\Sigma}_t\varepsilon_t \\ [\mathbf{0}]_{n(k-1)\times 1} \end{pmatrix}. \tag{10}$$

At time t, an exogenous shock ε_t affects the next state via F_t (the constant term υ_t does not affect the shock term). Thus, the effect of a unit-impulse on variable m after h time-steps is simply $F_{t+h}\dots F_{t+1}F_t$ times the unit-impulse vector where ε_t is substituted with zeroes everywhere except position m where it is 1 (the first n components gives the final state y_{t+h}). The IRF is given by:

$$IRF_t(h) = F_{h,t}\mathbf{A}_t^{-1}\boldsymbol{\Sigma}_t \tag{11}$$

where $[F_{h,t}]_{n\times n} = (F_{t+h}\dots F_{t+1}F_t)_{1:n,1:n}$ takes the first $n \times n$ block of the matrix product. The matrix $[IRF_t(h)]_{n\times n}$ gives the total impulse response; i.e., the response of a variable on a row given a shock of a variable on a given column.[8] The FEVD computed from orthogonalised

[6] Using the variance property of Gaussian processes.

[7] A detailed explanation of the posterior sampling technique of the parameters and hyper-parameters, along with their prior estimations, are given in Appendix B. Appendix C provides the visualisations of the posterior means of the model parameters and their corresponding convergence tests.

[8] To ensure stability, the $IRF_t(h)$ must decay to zero, i.e, be a stationary process with eigenvalues less than one.

IRFs are not order invariant (Lütkepohl, 2005). To overcome this issue, Diebold and Yilmaz developed the generalised FEVD (Diebold and Yilmaz, 2012) computed as:

$$\theta_{ij,t}(H) = \frac{\sigma_{j,t}^{-2} \sum_{h=0}^{H-1} (IRF_t(h) \cdot \Sigma_t' \cdot \mathbf{A}^{-1\prime})_{ij}^2}{\sum_{h=0}^{H-1} (IRF_t(h) \cdot IRF_t(h)')_{ii}}$$

where $(...)_{ij}$ represents component (i, j) in the matrix. FEVDs generated through orthogonalised impulse responses, normalise to one. However in the case of generalised FEVDs $\Sigma_{j=1}^{k} \theta_{ij,t}(H) \neq 1$. Normalising the FEVDs across the rows, satisfies the condition $\Sigma_{j=1}^{k} \tilde{\theta}_{ij,t}(H) = 1$. The normalised generalised FEVD is estimated as:

$$\tilde{\theta}_{ij,t}(H) = \frac{\theta_{ij,t}(H)}{\sum_{j=1}^{n} \theta_{ij,t}(H)} \tag{12}$$

The net pairwise directional spillover is given by:

$$VS_{ij,t}(H) = \tilde{\theta}_{ji,t}(H) - \tilde{\theta}_{ij,t}(H), \qquad i \neq j \tag{13}$$

When $VS_{ij,t}(H)$ is positive, market i is transmits volatility to market j, negative value indicates that market i is a receiver of volatility information from market j. For the case where $i = j$, we calculate the net volatility spillover from market i to all other markets via:

$$VS_{ii,t}(H) = \Sigma_{j=1,j\neq i}^{N} \tilde{\theta}_{ji,t}(H) - \Sigma_{j=1,j\neq i}^{N} \tilde{\theta}_{ij,t}(H). \tag{14}$$

When $VS_{ii,t}(H)$ is positive (negative), market i transmits (receives) volatility to (from) all other markets. From the definition it is also evident that $VS_{ii,t}(H)$ is the sum of $VS_{ij,t}(H)$ across all j for $i \neq j$

3.2. Portfolio construction strategies

Our study estimates the magnitude and directionality of volatility spillover indices amongst major commodity futures and the SPX. Highly interconnected sectors in a portfolio could exacerbate contagion risks when held concurrently during crises. Conversely, futures with limited volatility interactions could serve as alternative hedge assets. Assigning higher portfolio weights to futures with limited volatility interactions could yield more stable returns during periods of extreme uncertainty. We test our implications by constructing dynamic weighted portfolios of the selected nine commodity futures and SPX following the MCP (Broadstock et al., 2020) strategy. We compare the performance of the MCP strategy against the following baseline strategies — MVP (Markowitz, 1959) and EWP. In the interest of simplicity and to facilitate the extrapolation of implications, we restrict our analysis to long-only portfolios with no transaction costs.

3.2.1. Minimum connectedness portfolio

The MCP strategy Broadstock et al. (2020) minimises volatility spillover between assets within a portfolio. By reducing dependencies among the included assets, this approach enhances diversification, thereby the investment portfolio is able avoid severe drawdowns during market turmoil. To estimate the degree of interaction between variables on a bilateral level, we estimate the Pairwise Connectedness Index (PCI) given by:

$$PCI_{i,j,t}(H) = 2 * \left(\frac{\tilde{\theta}_{ij,t}(H) + \tilde{\theta}_{ji,t}(H)}{\tilde{\theta}_{ii,t}(H) + \tilde{\theta}_{ij,t}(H) + \tilde{\theta}_{ji,t}(H) + \tilde{\theta}_{jj,t}(H)} \right)$$

$$0 <= PCI_{i,j,t}(H) <= 1 \tag{15}$$

where $\tilde{\theta}_{ij,t}$ is the normalised FEVD (see Eq. (12)).[9] The strategy minimises volatility interconnectedness across the variables to build a portfolio more resilient to contagion shocks by assigning greater weight to less interconnected sectors over those with higher volatility interconnectedness. The weights are calculated using the following formula:

$$W_t = \frac{PCI_t^{-1} I}{I PCI_t^{-1} I} \tag{16}$$

[9] The $PCI_{i,j,t}$ matrix is symmetric and capable of reaching the global minimum in the convex optimisation problem.

Table 1
Entities used in the study.

Asset class	Data Source
Gold	Gold CME[a]
Silver	Silver CME[a]
Equity	S&P 500[b]
Crude Oil	WTI Crude[a]
Heating Oil	NY Harbor[a]
Natural Gas	Henry Hub[a]
Lumber	Lumber CME[a]
Copper	Copper CME[a]
Corn	Corn CME[a]
Wheat	Chicago SRW Wheat[a]

Rows 1–2 represent precious metals, row 3 represents equity, rows 4–6 represent energy, rows 7–8 represent industrial goods, rows 9–10 represent agriculture.

[a] Data sourced from *Datastream*.

[b] Data sourced from *Bloomberg*.

3.2.2. Minimum variance portfolio

The MVP strategy (Markowitz, 1959) strategy weighs sectors with lower covariances more heavily than those with higher covariances. We use the estimated time-varying conditional variance–covariance matrices from Eq. (7). The MVP weights are calculated as follows:

$$W_t = \frac{\mathbf{R}_t^{-1} I}{I \mathbf{R}_t^{-1} I} \tag{17}$$

3.2.3. Equally-weighted portfolio

The EWP strategy (DeMiguel et al., 2007) weighs all the constituent asset classes equally. The EWP weights are given by:

$$W_t = \frac{1}{N} \tag{18}$$

where N is the total number of asset classes.

4. Data

This study investigates fluctuations in the interconnectedness of weekly RV amongst major commodity futures and the US stock market across financial, economic and public health emergency-induced supply chain crises. We analyse nine highly traded commodity futures spanning key sectors: Energy, Agriculture, Precious Metals, and Industrial Goods (see Table 1)[10] The dataset comprises 1,938 weekly RV observations spanning over three decades, from January 1990 to February 2022.[11] This period includes several major economic crises, commodity price crashes, and the pandemic-induced crisis. For details on the crises covered in this study, see Table 2.[12]

Fig. 1 plots the price and return series of the data considered in the study. Gold, SPX and copper futures consistently depict an increasing

[10] Drawing on a comprehensive review of relevant literature (Rehman and Vo, 2021; Umar et al., 2021; Kang et al., 2017; Farid et al., 2021), we identify key commodity futures for our study, prioritising those with high market capitalisation, significant financialization, strong safe-haven attributes, and potential for intra-sector and inter-crisis variations. The selected futures represent some of the most actively traded commodities in their respective categories: Preciousmetals, Energy, Agriculture, Copper(Industrialgoods), Lumber(Industrialgoods).

[11] This analysis focuses on asset classes from the same geographical region, and by calculating weekly RV from daily closing prices, we minimise the impact of variations in trading hours. We appreciate the anonymous reviewer for suggesting this clarification.

[12] Justifications for the start and end dates of the crises are provided in Appendix A.1.

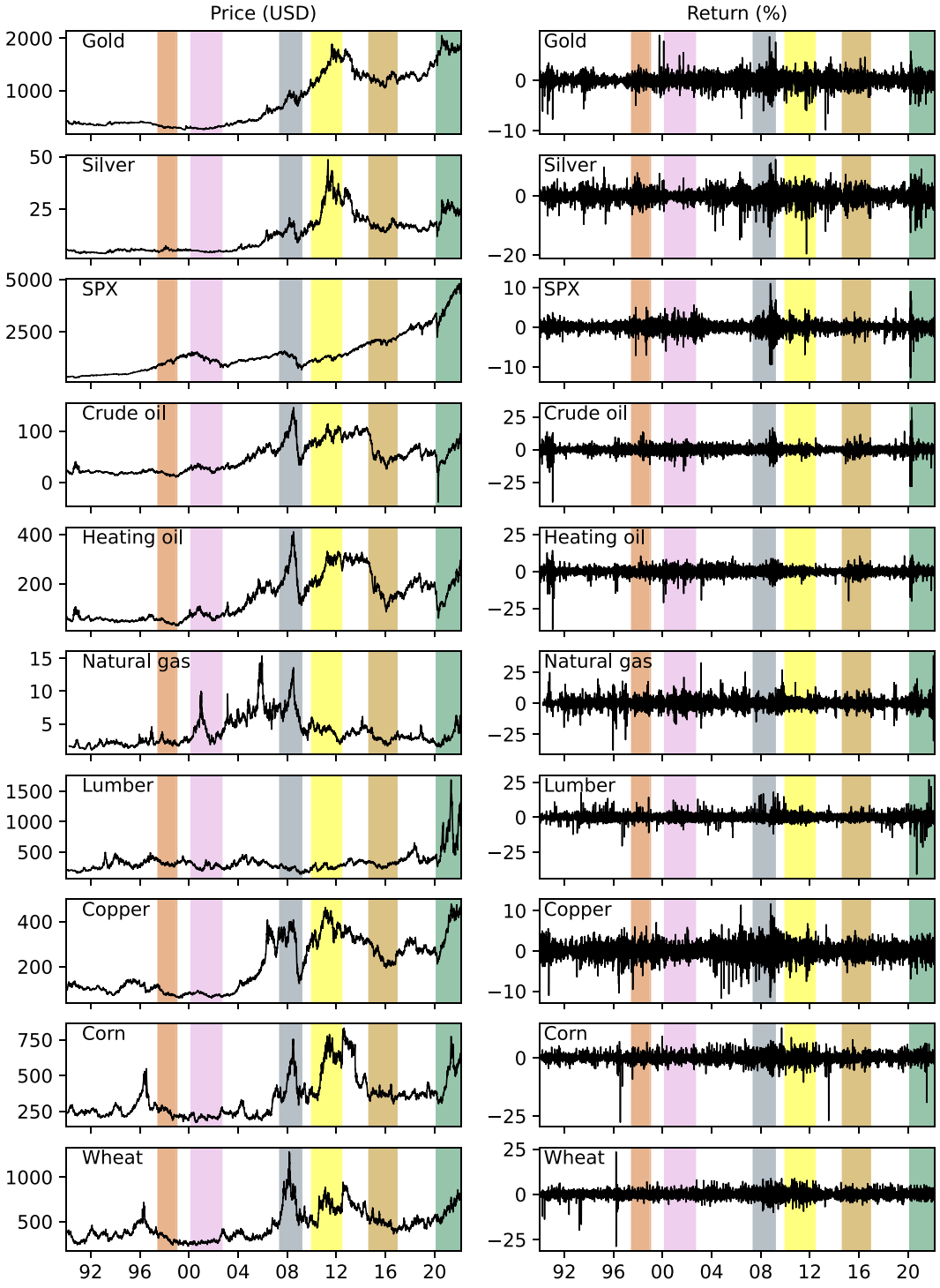

Fig. 1. Price and Return trends
The LHS of the figure plots the price trends for the asset classes under consideration in the study from Jan 1990 to Feb 2022. The various crisis periods are shaded as reported in Table 2. The RHS of the figure plots the return trends for the asset classes under consideration in the study from Jan 1990 to Feb 2022.

price trend. The prices of Natural gas futures declined significantly post-2009, coinciding with the glut in shale oil production (Kilian, 2016; Caporin and Fontini, 2017). Increased price volatilities correspond with extreme crisis events, especially after 2005. The return trends also exhibit higher variance during crisis periods. The COVID-19 crisis and the consequent lockdowns, in particular, had differing impacts on the prices of various futures. Lumber futures experienced historical price increases during the pandemic.[13] However, these rapid price

[13] Lumber futures traded at around $407 at the start of 2020 and hit a record high of $1670.50 in May 2021.

Table 2
Crises timeline.

Crisis event	Timeline
Asian Financial crisis	Jul 1997–Dec 1998
Dot-com bubble crash	Mar 2000–Oct 2002
Global Financial crisis	Jun 2007–Feb 2009
European Sovereign Debt crisis	Jan 2010–May 2012
Oil price crash	Sep 2014–Nov 2016
COVID-19 pandemic crisis	Mar 2020–Feb 2022

This table indicates the range of dates for the various crises considered in the study. Figs 1 to 10 will follow the shading scheme as represented in this table to differentiate the various crises.

increases were more indicative of pent-up demand from a previously under-inventoried sector and inflationary pressures than actual growth. Subsequently, prices declined significantly,[14] further increasing their volatility. Crude oil futures, on the other hand, experienced massive price drops at the onset of the crisis[15] before experiencing massive price hikes later, with economies re-opening and further increasing volatility.

Table 3 depicts the descriptive statistics of the RVs for the nine commodity futures and SPX for the overall data from Jan 1990 to Feb 2022.[16] Energy futures and SPX have the widest range in their RVs. The skewness and kurtosis results indicate that the data series for the RVs of all the asset classes are positively skewed and fat-tailed, implying the existence of a high proportion of high-volatility events. The Jarque–Bera test statistics are consistent with the data series drawn from a non-normal distribution.

5. Results

5.1. Analysing the time-varying characteristics of realised volatility and stochastic volatility

Realised Volatility (RV) is the second-order moment-based measure defined as the squared root of the sum of weekly squared returns (see Eq. (1)). We aim to assess the interconnectedness between major commodity futures and the SPX by quantifying the transfer of RV, providing insights into shared volatility exposures across these asset classes. The LHS of Fig. 2 plots the weekly RV of the selected commodity futures and the SPX index from Jan 1990 to Feb 2022. We highlight the major crisis periods across the plots as mentioned in Table 2. The RV plot gives us an insight into the extent of price fluctuations across various futures and the SPX index. Generally, we observe heightened fluctuations in the RV values of the futures and equity index corresponding to different crisis periods. Coinciding with the Gulf War of 1990–91 and the resultant embargo on Iraq and Kuwait, crude oil futures exhibit significant perturbations in the RV. Crude oil prices doubled within a few months until Saudi Arabia intervened to restore world oil production by November 1990 (Hamilton, 2011). The RV trends for natural gas, copper and wheat futures show significant volatility around 1996 (as seen by the spikes before the AFC), coinciding with the Enron collapse and the subsequent decline in the trading of natural gas futures (Pindyck, 2004).

The GFC marked a period of heightened volatility in the RV values for major equity indices and commodity futures. Financialisation of commodity futures, particularly energy futures, increased the risk of potential contagion effects as shocks from the equity markets affect commodity markets and vice versa (Wen et al., 2012; Nguyen et al., 2020; Wang et al., 2021). Even precious metal futures like gold and silver display considerable volatility owing to increased "flight to quality" behaviour by speculators/investors exacerbated by overall uncertainty and liquidity concerns (Klein, 2017; Miyazaki and Hamori, 2013).

Energy futures experience another increase in volatility during the price slump from 2014 to 2016. This was primarily due to a supply glut caused by increased technological efficiency in shale gas production and OPEC's refusal to restrain production, leading to a more than 70% reduction in oil prices (Zhang et al., 2017; Fantazzini, 2016; Gong et al., 2021). Consequently, the RV trends for energy futures during this period were marked by heightened volatility.

The COVID-19 pandemic-induced lockdowns from March 2020 again created a highly chaotic situation with varying impacts on different futures. Prices of energy futures plummeted. The RV trends for crude oil and heating oil futures capture the chaos brought about by historical lows in oil futures' prices. In contrast, the RV trends of corn and lumber futures capture the increased volatility in their prices brought about by massive price increases caused by supply chain disruptions.

To estimate the magnitude and direction of the spillover effects, we feed the RV data into our TVP-VAR-SV model as given in Eq. (5). Details of prior selection and calculation of the posterior means are provided in Appendix B. The TVP-VAR-SV model outputs the posterior means for the time-varying parameters $\hat{\alpha}_t$, $\hat{\beta}_t$ and $\hat{h}_t$, which capture the time-variation in the contemporaneous terms, the lag propagation and the impact of the exogenous shocks affecting the model system respectively.

The RHS of Fig. 2 plots the SV component of the model $\hat{h}_t$ for the different futures and SPX. By incorporating the time-varying SV term, we account for the dynamic variances in the exogenous shocks that impact the model system. Standard VAR and TVP-VAR models assume homoskedastic (constant) variances for the intrinsic Gaussian noise terms across the entire time period (McMillan and Speight, 2010; Bouri et al., 2021b). Our SV plots show that allowing for time variation in the variances of the exogenous shock terms (heterogeneity) better captures the dynamic nature of the exogenous model shocks. We observe substantial spikes in the SV term corresponding with various crisis periods. For instance, the significant perturbation in $\hat{h}_t$ in crude and heating oil futures during the onset of the COVID crisis coincides with the largest drop in energy futures prices in history.

Modelling time-varying error variances helps us understand the differences in the nature of shocks and their varying impact on different futures. While economic crises like GFC and ESDC primarily increase variation in volatility levels of energy futures, precious metal futures and SPX, the pandemic-induced crisis and the resulting supply chain disruptions affected other commodity futures that were so far isolated from shocks in the energy futures or equity market. Our results capture the unique impact on lumber futures' volatility (as seen by the increase in its SV value) that was not necessarily observed during previous crisis periods. This analysis reiterates the importance of capturing the heteroskedasticity in error variances while accounting for time-variation within the VAR model (Sims and Zha, 2006; Koop, 2011; Chan and Eisenstat, 2018).

5.2. Analysing the time-varying directional volatility spillover indices

We calculate the net pair-wise volatility spillover indices to observe the direction and magnitude of volatility transmissions across major commodity futures and SPX. We use the generalised FEVD based spillover index (developed by Diebold and Yilmaz, 2008, 2012) as explained in Section 3.1.1. Eq. (13) calculates the time-varying net pair-wise directional spillover index from commodity future i to commodity future j. Eq. (14) calculates the time-varying net spillover index from commodity future i to the remaining commodity futures. To determine the optimal forecasting horizon, we compute the net pair-wise and overall net spillover indices for horizons from H = 1 to 16. We select

[14] Lumber futures prices fell by 64% to trade at around $410 in September 2020, trading at pre-COVID levels again.

[15] On April 20, 2020, WTI crude oil futures saw the largest drop in history when its prices dropped by 306% and settled at −37.63$ a barrel.

[16] Tables A.6–A.16 provide detailed descriptive statistics for the dataset, segmented by each specific crisis considered in the study.

Table 3
Descriptive Statistics.

Asset class	Mean	Median	Min	Max	Skew	Kurtosis	Jarque–Bera Test
Gold	6.13	5.34	0.44	36.11	2.09	8.11	6723.51***
Silver	10.82	9.09	0.72	72.55	2.21	8.52	7432.95***
SPX	6.6	5.45	0.52	81.79	4.51	40.41	138424.23***
Crude oil	13.61	11.74	0.71	211.04	6.99	98.25	795204.78***
Heating oil	12.56	11.17	1.89	122.35	3.44	31.19	82392.38***
Natural gas	15.4	14.54	0.0	89.13	1.04	3.4	1286.13***
Lumber	11.99	11.47	0.72	50.13	1.2	3.58	1499.14***
Copper	9.03	8.29	0.0	55.85	1.57	6.29	3990.0***
Corn	9.35	8.12	0.45	41.95	1.52	3.35	1654.75***
Wheat	10.81	9.64	1.28	54.88	1.85	6.62	4644.72***

This table presents the descriptive statistics for the Realised Volatility (RV) of the asset classes considered in the study from Jan 1990–Feb 2022. The Jarque–Bera test is for the following significance levels: *** indicates significance at 1% level, ** indicates significance at 5% level and * indicates significance at 10% level.

H = 8 as the optimal horizon, as spillover values stabilise at their steady-state maximum beyond this point.[17]

We plot the spillover indices in Fig. 3, where we have again highlighted the crisis periods. The lines are red in regions where the values are positive, while being blue otherwise. The off-diagonal plots show the net pair-wise spillover index as defined in Eq. (13), where a red (blue) line implies that the row asset class transmits (receives) volatility onto (from) the column asset class. We note that the off-diagonals mirror one another up to a sign of −1 by symmetry. The diagonal plots show the net volatility spillover to the remaining asset classes defined in Eq. (14), where a red (blue) line implies that the asset class transmits (receives) volatility in net to (from) all other asset classes considered in this study.

Our results indicate that the nature of spillovers is not static for the period under consideration. Commodity futures continually interact with other futures/SPX by transmitting/ receiving volatility information. The nature of inter-relationships is dynamic and prone to change. Commodity futures that transmit volatility information in some periods become net receivers of volatility information in others. During crises, spillover of volatility information can potentially exacerbate, sometimes impacting commodity futures that previously had minimal interactions with the transmitting asset class. Volatility transmitting asset classes exert significant influence to the receiver, propagating risks and potentially triggering contagion effects during crises. Conversely, volatility receivers must account for their sensitivity to external factors when evaluating future performance.

SPX is the dominant volatility transmitter in our model, primarily affecting crude and heating oil futures. During crises, these transmissions intensify, highlighting potential contagion effects. Historically, heightened volatility in SPX has consistently led to increased transmission effects to crude and heating oil futures, as corroborated by existing studies (Mensi et al., 2021d; Asadi et al., 2022). During crises, investors often flock to more stable assets, resulting in increased volatility transmissions to precious metals futures (Farid et al., 2021; Umar et al., 2021; Kang et al., 2017). Additionally, our results indicate that copper, lumber, and wheat futures also predominantly transmit volatility, while gold, crude oil, and corn futures predominantly receive volatility. Silver and heating oil futures alternate between being net transmitters and receivers of volatility information. Natural gas futures are predominantly net transmitters of volatility but continually receive volatility from lumber futures. The COVID-19 pandemic-induced lockdowns however led to a complete shutdown of production processes, exacerbating the volatility in the already under-inventoried lumber sector. This resulted in record levels of volatility transmission from lumber to natural gas futures during this period, causing natural gas futures to completely transition to net receivers of volatility. Understanding inter-asset interconnectedness is thus essential for market practitioners and policymakers to accurately gauge potential sensitivity risks that a particular asset class might face.

To measure the differences in impacts of volatility spillover contribution to/from the futures/SPX across various crises, we calculate the average volatility spillover contributed to/from commodity future i from/to the remaining asset classes j during a particular crisis using

$$Contrib_{i,j}(H) = \left| \frac{1}{T} \sum_{t=1}^{T} \frac{VS_{ij,t}(H)}{\sum_{j \neq i} \left| VS_{ij,t}(H) \right|} \right| \quad i \neq j, H = 8, T = [crisis\ period] \tag{19}$$

where $VS_{ij,t}(H)$ is the net volatility spillover from(to) market i to(from) market j when the value is positive(negative). Sections 5.2.1 to 5.2.5 contain bar plots representing the sector-wise average volatility spillover contribution across crises. The bar plots are colour-coded to represent various crises consistent with Table 2. The positive(negative) signs on the bar plots indicate if a particular asset class is a net transmitter (receiver) of volatility during a particular crisis.

5.2.1. Volatility spillovers of precious metal futures

We consider gold and silver futures to represent the precious metals sector. Theory suggests that precious metals futures serve as hedge assets, insulating investors/speculators from global financial volatility by propagating a "flight to quality" behaviour, increasing the demand for precious metals during extreme risk scenarios (Klein, 2017; Miyazaki and Hamori, 2013). We hypothesise that precious metal futures are dominant receivers of volatility information with spillovers deepening, especially during crises.

Despite this reasoning, gold futures were predominantly a net transmitter of volatility until the mid-2000s, transmitting significant volatility information to energy futures like crude and heating oil as seen in Fig. 3 (1R4C and 1R5C)[18] Volatility transmissions from gold to crude and heating oil futures extended during both the AFC and DBC.

Gold futures however consistently receive volatility from SPX keeping in line with the "safe-haven asset" perception (Bouri et al., 2021a; Buccioli and Kokholm, 2021; Mensi et al., 2021d). We observe heightened volatility transmissions from SPX to Gold futures (28%) on average during the dotcom bubble crash[19] (see Fig. 4). Post-2005, gold futures transition to become net receivers of volatility with spillovers exacerbating during crises. As shown in Fig. 4, gold receives substantial volatility information on average from SPX(22%), natural gas (17%) and silver (17%) during the GFC. During the oil price crash, Gold futures receive significant volatility from SPX (32%) and Natural gas futures (14%) whilst still transmitting volatility to Copper (16%) and Corn futures (12%). Similarly, during COVID, gold futures receives significant volatility information on average from SPX (21%), natural gas (17%) and transmits volatility to corn futures (18%). Our results

[17] Details of horizon saturation are given in Appendix C.1.

[18] Note: 1R4C refers to the first row and fourth column of Fig. 3.

[19] The Dotcom crash saw close to 800 internet based companies going bankrupt with SPX losing nearly 49% of its value (Rovenpor, 2003).

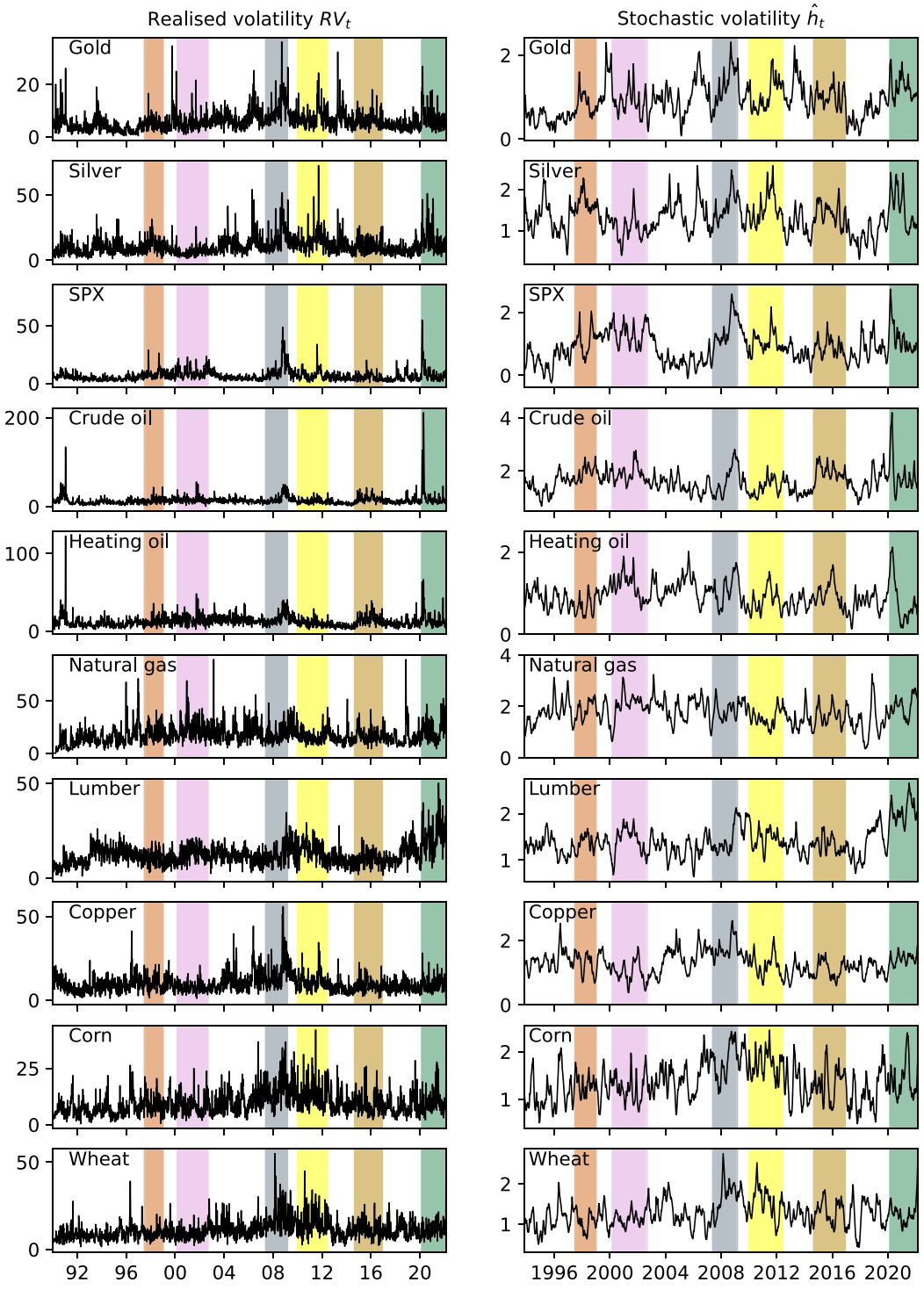

Fig. 2. Realised Volatility and Stochastic Volatility ($\hat{h}_t$)
The LHS of the Figure plots the realised volatility of the asset classes under consideration in the study from Jan 1990 to Feb 2022. The various crisis periods are shaded as reported in Table 2. The RHS of the Figure plots the stochastic volatility component from the TVP-VAR-SV model from Nov 93 to Feb 2022, excluding the data period considered for training the priors of the model ($\hat{h}_t = \exp(\log \hat{\sigma}_t)$).

align with literature alluding to gold futures being a net receiver of volatility information due to functioning as a safe haven asset (Balcilar et al., 2019; Mensi et al., 2017, 2021a; Bouri et al., 2021a).

Silver is a more robust transmitter of volatility than gold until the mid-2000s. For instance, we observe in Fig. 3 that, from Mar 95 to May 95, silver transmits close to 33% of its volatility to SPX (2R3C), 15% of its volatility to corn (2R9C), 16% to wheat (2R10C) and 10% to copper (2R8C). Silver ceases to be a transmitter of volatility to SPX after this period and transitions completely to become a net receiver of volatility from SPX . Silver futures transmit significant volatility information on average to agricultural futures during AFC and Oil price crash and COVID (see Fig. 4). Our results also highlight the dynamic nature of integration that silver shares with other energy and industrial futures. Silver and copper alternate between transmitting/receiving volatility to/from each other (consistent with Qiao and Han, 2022). Natural gas, lumber and SPX remain net transmitters of volatility information to

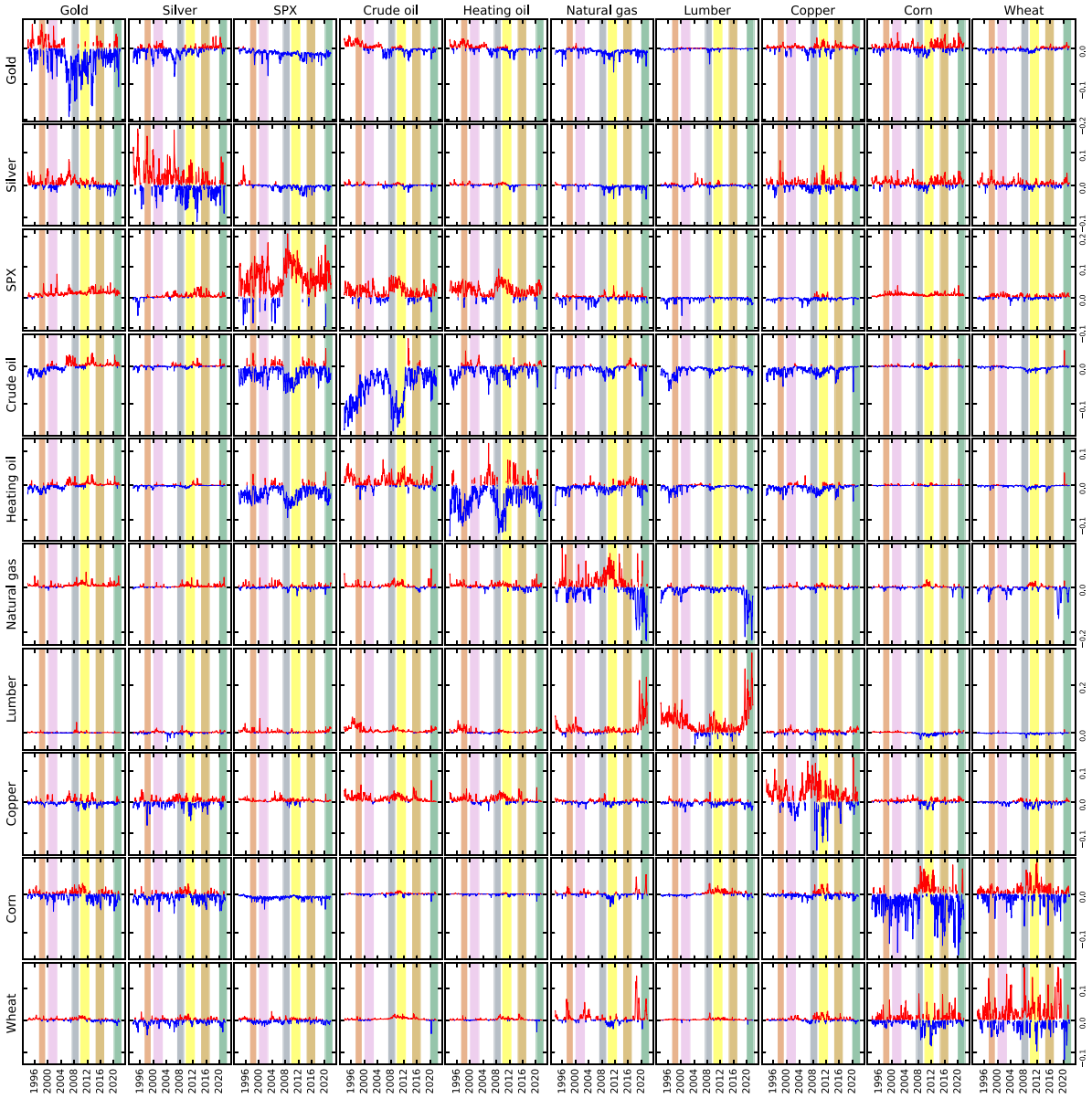

Fig. 3. Net pair-wise volatility spillover index
The Figure illustrates the net pairwise spillover index for variance decomposition period H= 8. Details of the shaded crisis periods are mentioned in Table 2. The X axes show the dates from Nov 93 to Oct 2021. The Y axes show the extent of volatility spillover. The red lines represent positive net spillover (net transmitter) from row i to column j. The blue lines represent negative net spillover (net receiver) from row i to column j. The off-diagonal elements plot the net pairwise spillover index defined in Eq. (13). The diagonal elements plot net volatility spillover to the remaining asset classes defined in Eq. (14). The off-diagonals mirror one another up to a sign of −1. (For interpretation of the references to colour in this figure legend, the reader is referred to the web version of this article.)

silver (consistent with Mensi et al., 2017 and Farid et al., 2021).

5.2.2. *Volatility spillovers of SPX*

SPX is a leading indicator variable to forecast volatility changes in crude oil, heating oil and gold futures consistent with Farid et al. (2021), Wang and Wu (2018) and Balcilar et al. (2018). Despite that, SPX experiences brief periods where it transitions to become a net receiver of volatility information. From March to May 95, there is a one-off perturbation in volatility transmission from silver to SPX (36%) (see Fig. 3 (3R2C).[20])

Volatility transmissions from SPX are exacerbated during various crises, further cementing the significance of accounting for volatility transmissions from SPX in studies primarily focused on commodity futures. The integration between crude and heating oil with SPX exacerbates during crises post-2004, alluding to the increasing financialisation of energy futures and the consequent contagion shocks from SPX (see Fig. 5) (Mensi et al., 2021d). Volatility transmissions from SPX reached historical levels on Sep 08, transmitting about 32% volatility to crude oil and 46% volatility to heating oil futures. During the onset of the pandemic, SPX remained a net transmitter of volatility information. However, coinciding with the largest drop in oil futures prices in Apr 2020, SPX briefly transitions to become a net receiver of volatility, receiving volatility information from crude (24%) (see Fig. 3 3R4C) and heating oil futures (17%) (see Fig. 3 3R5C).

[20] Note: 3R2C refers to the third row and second column of Fig. 3.

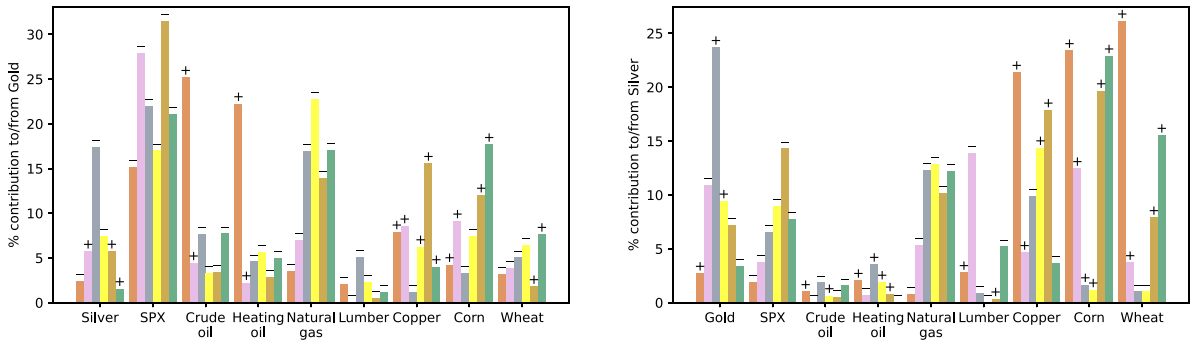

Fig. 4. Average volatility spillover contribution to/from precious metal futures during crises.
The colours represent different crises given in Table 2: AFC, DBC, GFC, ESDC and COVID. The X-axes indicate the commodity futures/SPX that are in net transmitting/receiving volatility to/from the precious metal future. The percent contribution of mean volatility spillover is given in Eq. (19). The + sign indicates that the precious metal future was in net transmitting volatility to that future/SPX during that particular crisis period. The − sign indicates that the precious metal future was in net receiving volatility from that future/SPX during that particular crisis period. (For interpretation of the references to colour in this figure legend, the reader is referred to the web version of this article.)

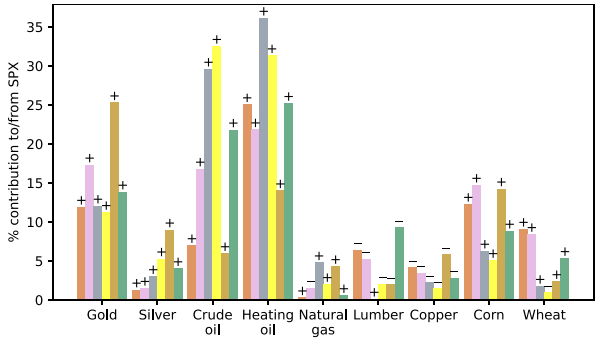

Fig. 5. Average volatility spillover contribution proportion to/from SPX during crises.
The colours represent different crises given in Table 2: AFC, DBC, GFC, ESDC and COVID. The *X*-axis indicates the commodity futures that are in net transmitting/receiving volatility to/from SPX. The percentage contribution of mean volatility spillover is given in Eq. (19). The + sign indicates that the SPX was in net transmitting volatility to that future during that particular crisis period. The − sign indicates that SPX was in net receiving volatility from that future during that particular crisis period. (For interpretation of the references to colour in this figure legend, the reader is referred to the web version of this article.)

Overall, SPX continues to be deeply integrated with gold and oil futures, transmitting significant volatility information to them. Natural gas futures have, however, remained isolated from volatility shocks from SPX, making them an exciting hedging alternative. Our results align with Jebabli et al. (2022) and Niu and Hu (2024) who report limited interactions between natural gas futures and SPX and support the hedging abilities of natural gas futures against shocks in SPX.

5.2.3. *Volatility spillovers of energy futures*

We consider crude oil, heating oil and natural gas futures to represent the energy sector in our study. The financialization of energy futures has made crude oil and heating oil more vulnerable to stock market fluctuations. Similarly, the increased speculative investment in energy futures has ensured that periods of heightened volatility in energy futures coincide with extreme volatility shocks in equity markets (Creti and Nguyen, 2015; Yang et al., 2024).

Our results indicate that crude oil futures are predominantly a net receiver rather than a transmitter of volatility information (see Fig. 3 4R4C). They predominantly receive volatility information from other energy, industrial futures and SPX. In the aftermath of the 1991 Gulf War, crude oil futures remained especially susceptible to volatility shocks from other energy futures despite oil production reaching previous levels. Between Nov 93 and Mar 96, crude oil futures experienced record levels of volatility spillover from heating oil (25%) (4R5C),[21] SPX (20%) (4R3C), lumber (16%) (4R7C), gold (15%) (4R1C) and copper futures(14%) (4R8C). The GFC, further heightened volatility dependence of crude oil futures, reaching unprecedented levels by Sep 08. From Sep 08 to Aug 10, crude oil received 38% of its volatility information from SPX (4R3C), 17% from copper (4R8C), 12% from lumber (4R7C) and 12% from natural gas (4R6C). Crude oil remained net receivers of volatility during the 2014–16 oil price crash despite transmitting around 12% volatility information to natural gas futures (see Fig. 6) . During the onset of the COVID-19 pandemic, coinciding with the largest single-day price drop in oil futures in April 2020, crude oil futures, transition from net receiver to transmit around 19% volatility to SPX (4R3C). These results are in line with Corbet et al. (2021), who document the transition of crude oil futures from net receivers to net transmitters of volatility to the SPX during the early stages of the pandemic. Our results align with literature that find strong integration between crude oil futures and stock market indices with crude oil futures predominantly behaving as net volatility receivers (Gong et al., 2021; Xu et al., 2019, 2024; Mensi et al., 2021b).

Like crude oil futures, heating oil futures primarily function as net receivers of volatility information (see Fig. 3 row 5). Heating oil futures however, consistently transmit volatility to crude oil futures. The brief periods where heating oil transition to become overall net volatility transmitters are due to substantial volatility transmissions to crude oil futures. For instance, heating oil transmits close to 60% of its volatility information to crude oil during August 2005 (5R4C). Our results are consistent with Gong et al. (2021). We observe a pattern where heating oil futures are brief net transmitters of volatility at the onset of various crises before becoming net receivers of volatility. From April 2008 to January 2011, heating oil futures receive about 44% volatility from SPX (5R3C), 17% from copper (5R8C) and 12% from natural gas futures (5R6C). Similarly, during the pandemic-induced crisis, heating oil futures again transition to become net receivers of volatility. From August 2020, they receive about 54% volatility information from SPX (5R3C) and 15% from lumber futures (5R8C). Heating oil futures remained net receivers of volatility during the 2014–16 oil price crash despite transmitting around 18% volatility information to natural gas futures (see Fig. 6)

Our findings provide strong evidence for the financialisation of energy futures, such as crude oil and heating oil, and the resulting intensification of volatility spillovers from SPX during various crises (Mensi et al., 2021d; Balcilar et al., 2018). Crude oil futures also absorb substantial volatility from other energy and industrial futures

[21] Note: 4R5C refers to the fourth row and fifth column of Fig. 3.

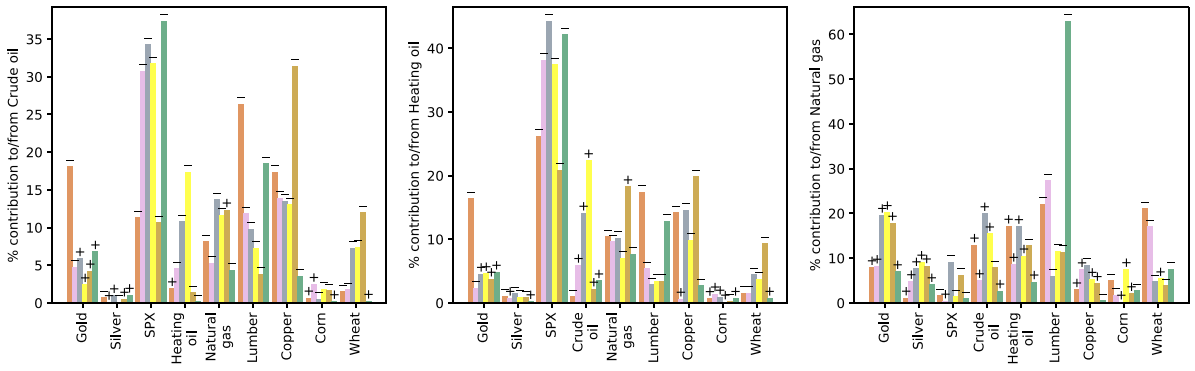

Fig. 6. Average volatility spillover contribution to/from Energy futures during crises.
The colours represent different crises given in Table 2: AFC, DBC, GFC, ESDC and COVID. The X-axis indicates the commodity futures/SPX that are in net transmitting/receiving volatility to/from the energy future. The percentage contribution of mean volatility spillover is given in Eq. (19). The + sign indicates that the energy future was in net transmitting volatility to that future/SPX during that particular crisis period. The − sign indicates that energy future was in net receiving volatility from that future/SPX during that particular crisis period. (For interpretation of the references to colour in this figure legend, the reader is referred to the web version of this article.)

included in the study. While heating oil is a net volatility transmitter to crude oil, it also receives considerable volatility from natural gas and industrial futures.

Unlike crude and heating oil futures, natural gas futures consistently transmit volatility until Dec 2016 (see Fig. 3 row 6). Our results indicate that natural gas futures do not experience substantial integration with SPX and are relatively isolated from volatility shocks affecting the SPX market (like the DBC or GFC). Natural gas futures also do not exhibit significant within-energy sector volatility integration compared to crude oil-heating oil future integration. Our findings are consistent with studies that the prices of natural gas futures have decoupled from crude and heating oil prices (Mensi et al., 2021c; Erdős, 2012; Ramberg and Parsons, 2012; Gong et al., 2021). Since December 2016, natural gas futures have become significant recipients of volatility spillovers, particularly from lumber. During the initial phase of the COVID-19 crisis in April 2020, natural gas briefly shifted to being a net transmitter of volatility, notably to crude oil (23%) (6R4C) and heating oil (18%) (6R5c). However, despite this short-lived shift, the broader pandemic period was marked by an exceptionally high reception of volatility from lumber, averaging 63%. The pandemic-induced lockdowns, which severely disrupted manufacturing and industry, further intensified these spillovers from lumber futures (see Fig. 6).

5.2.4. Volatility spillovers of industrial futures

In this study, we use lumber and copper futures to represent the industrial sector. Lumber is predominantly a net transmitter of volatility information. From Fig. 3 row 7, we observe that lumber experienced historical levels of volatility transmission from February 2019, coinciding with soaring levels of RV and SV (see Fig. 2). Lumber futures transmit substantial amounts of volatility information to natural gas futures. Even before the onset of the COVID-19 crisis, from February 2019 to February 2020, lumber transmitted about 68% of its volatility information to natural gas (see Fig. 3 7R6C[22]). During the COVID crisis, lumber futures transmit close to 65% of their volatility information to natural gas (see Fig. 7). Our results reaffirm findings of increased integration between lumber and natural gas due to their use in manufacturing activities. Shocks in lumber markets propagate to increase volatility in natural gas prices.

Copper, a key industrial commodity, consistently acts as a net transmitter of volatility, particularly to crude and heating oil futures. We observe substantial transmission spikes from copper to crude oil (15%) (see Fig. 3 8R4C), heating oil(16%) (8R5C) and silver(17%) futures (8R2C) from May 06 to June 08. As illustrated in Fig. 7, copper typically transmits most of its volatility to crude and heating oil on average during crises. Copper futures have a more dynamic relationship with natural gas and lumber futures, with copper alternating between being a transmitter or receiver for different crises. However, the volatility chaos caused by the pandemic in lumber futures led to copper receiving historically high levels of volatility from lumber, averaging to around 26%.

5.2.5. Volatility spillovers of agricultural futures

In this study we use corn and wheat futures to represent the agricultural sector. Fig. 3 shows that corn and wheat futures are characterised by strong bidirectional within-sector volatility transmissions.

For the most part, corn futures are an active receiver of volatility information. They primarily receive volatility from silver, gold and SPX. However, as shown in Fig. 3 row 9, from June 2008 to October 2012, coinciding with the GFC and ESDC, corn futures significantly transmit volatility to other asset classes, predominantly wheat, gold, silver, copper and lumber futures while also periodically transitioning to receive volatility from them. On average, during the GFC, corn receives 16% volatility from SPX while transmitting close to 10% volatility to lumber and 8% to wheat (see Fig. 8). During COVID, corn receives heightened volatility transmission on average from gold (17%), silver (22%), SPX (14%) and copper (9%) while transmitting close to 10% volatility information on average to natural gas futures.

Wheat futures periodically transition between net transmitters and receivers of volatility information, although the extent of transmissions is greater. Corn and natural gas futures actively engage with wheat futures. As shown in Fig. 8, wheat futures consistently transmitted volatility to gold barring the pandemic-induced crisis. Wheat receives significant proportion of its volatility from silver on average during the AFC(26%) and COVID (23%). Barring ESDC, wheat transmits a substantial amount of its volatility on average to natural gas (especially during AFC(22%) and COVID (23%)). During periods of crises, wheat predominantly receives volatility signals from corn. Overall, our results align with Farid et al. (2022) and Mensi et al. (2021d) who document significant interactions between agricultural, energy, precious metal and industrial futures.

5.3. Noteworthy aspects of volatility transmissions across different crises

In our analyses, we identify some consistent patterns across various crises and some specific fluctuations that correspond to the unique characteristics of each crisis. Recognising these trends can be significant for optimising portfolios and enhancing risk management strategies.

Our results are consistent with SPX being the largest net transmitter of volatility (Farid et al., 2021; Bouri et al., 2021b). We also find

[22] Note: 7R6C refers to the seventh row and sixth column of Fig. 3.

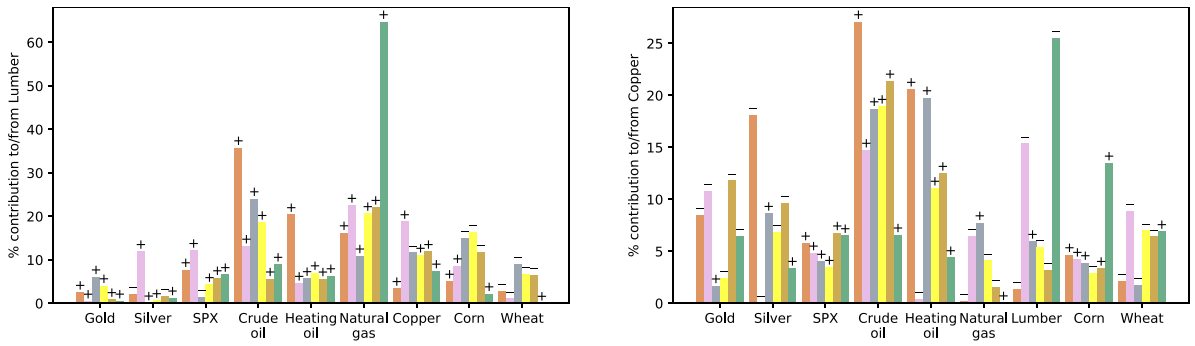

Fig. 7. Average volatility spillover contribution to/from Industrial futures during crises.
The colours represent different crises given in Table 2: AFC, DBC, GFC, ESDC and COVID. The X-axis indicates the commodity futures/SPX that are in net transmitting/receiving volatility to/from the industrial future. The percentage contribution of mean volatility spillover is given in Eq. (19). The + sign indicates that the industrial future was in net transmitting volatility to that future/SPX during that particular crisis period. The − sign indicates that the industrial future was in net receiving volatility from that future/SPX during that particular crisis period. (For interpretation of the references to colour in this figure legend, the reader is referred to the web version of this article.)

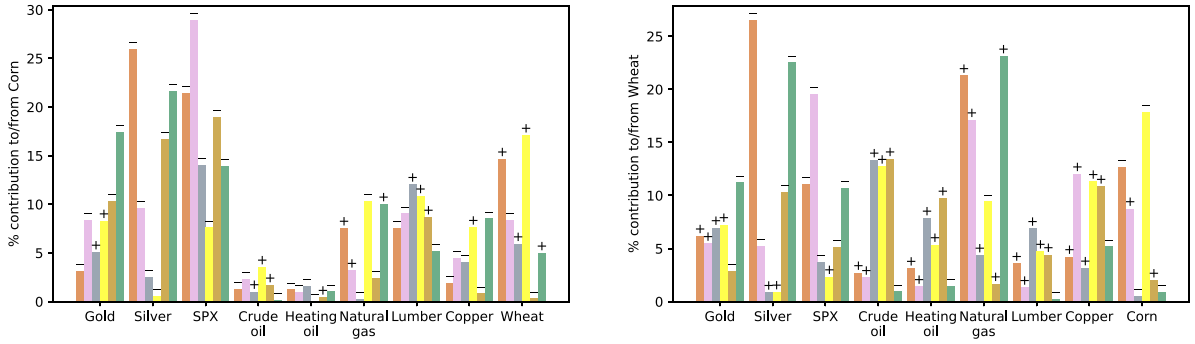

Fig. 8. Average volatility spillover contribution to/from Agricultural futures during crises.
The colours represent different crises given in Table 2: AFC, DBC, GFC, ESDC and COVID. The X-axis indicates the commodity futures/SPX that are in net transmitting/receiving volatility to/from the agricultural future. The percentage contribution of mean volatility spillover is given in Eq. (19). The + sign indicates that the agricultural future was in net transmitting volatility to that future/SPX during that particular crisis period. The − sign indicates that agricultural future was in net receiving volatility from that future/SPX during that particular crisis period. (For interpretation of the references to colour in this figure legend, the reader is referred to the web version of this article.)

evidence of increasing contagion effects from SPX to energy futures. SPX consistently transmits volatility information to crude and heating oil futures, deepening spillovers during crises. Volatility shocks to SPX translate to volatility shocks in crude and heating oil futures. Our results add to existing literature that points to the *financialisation* of energy futures and the subsequent reduction in diversification potential offered by crude and heating oil futures (Bianchi et al., 2020; Main et al., 2018; Basak and Pavlova, 2016; Nguyen et al., 2020). We also allude to the importance of incorporating equity indices in studies involving volatility spillover analyses of energy futures.

Gold futures function as safe-haven assets, shielding speculators from periods of heightened volatilities in both SPX and energy futures. Nguyen et al. (2020) find that gold futures remain negatively correlated to shocks in both equity and oil markets. Its supply scarcity and ability to hold value further make gold futures ideal hedge assets. Our results substantiate the safe-haven characteristic by finding evidence for increasing volatility spillover information received by gold futures from SPX and energy futures, exacerbating during crises (Balcilar et al., 2019; Mensi et al., 2017, 2021a; Bouri et al., 2021a). We, however, observe more muted overall volatility transmissions to gold during the pandemic-induced crisis than earlier crises (see Fig. 3 1R1C). Despite record stock market lows at the onset of the pandemic, immediate governmental intervention, coupled with rising hedging costs and historical evidence of significant reductions in prices of gold investments following crises, could have contributed to the reduced "flight to quality" towards gold. Several other studies concur with the dissipating notion of gold as safe-haven assets post the COVID crisis (Burdekin and Tao, 2021; Akhtaruzzaman et al., 2021; Baur and Trench, 2022).

Our study reveals that crude oil futures predominantly act as a net receiver of volatility information, amplifying notably during crises such as the aftermath of the 1990–91 oil crisis and the GFC. During these periods, crude oil futures experienced heightened volatility levels, drawing significant cues from heating oil, SPX, and natural gas markets. Our results are consistent with Gong et al. (2021), who find that crude oil futures predominantly receive volatility from both heating oil and natural gas futures. During the oil price crash however, crude and heating oil futures transmit volatility to natural gas futures, though the overall impact on natural gas was less pronounced. Notably, at the onset of the COVID-19 pandemic, crude oil futures briefly became an overall net transmitter of volatility, coinciding with the sharpest recorded drop in oil futures prices. Following this period, crude oil futures reverted to their role as a net receiver for the rest of the pandemic. These results are in line with Corbet et al. (2021), who document the transition of crude oil futures from net receivers to net transmitters of volatility to the SPX during the early stages of the pandemic. It is worth noting that the level of volatility information received during the pandemic was comparatively more subdued than during the GFC.

Natural gas futures remain isolated from volatility shocks in SPX. They also do not have significant interactions with crude and heating oil futures. We posit that natural gas futures could be an exciting hedge to protect from volatility shocks in SPX and crude and heating oil futures during both crises and non-crises. Our findings align with that of Okhrin et al. (2023) who report the predictive influence SPX and natural gas have on the crude oil market. Our findings also align with other studies (Mensi et al., 2021c; Rizvi et al., 2022), further affirming their potential as a hedging asset. Our results are consistent

with studies alluding to the decoupling of natural gas future prices from other energy futures owing to the US shale gas revolution (2008) and the subsequent shift from oil-based pricing (Ramberg and Parsons, 2012; Erdős, 2012; Zhang and Ji, 2018). Similarly, agricultural futures do not have significant interactions with SPX and crude and heating oil futures during crises and non-crises and could serve as an avenue for risk diversification (Yip et al., 2020).

This study differentiates the impact of volatility transmissions amongst asset classes depending on the nature of various crises. An economic crisis like the GFC is characterised by exacerbated transmissions from SPX to energy futures due to exposure to common shocks and from SPX to precious metal futures as investors scramble to invest in more stable hedge assets. In contrast, the pandemic-induced crisis uniquely heightened spillovers from lumber to natural gas futures unobserved during previous crises. Production cuts and lockdowns severely impacted volatility transmissions across industrial, natural gas and agricultural futures. The pandemic-induced crisis was more pervasive than previous crises regarding exacerbated volatility transmissions.

5.4. Portfolio analysis

Analysing the direction and magnitude of volatility interconnectedness has important portfolio ramifications as highly integrated sectors could exacerbate overall portfolio risk during crises. The MCP strategy introduced by Broadstock et al. (2020) reduces portfolio risk by minimising bilateral volatility transmissions between assets. It does so by allocating greater weight to less interconnected sectors, thereby reducing dependence on highly integrated sectors. We compare historical performance of the MCP strategy against the conventional MVP and EWP strategies similar to the following papers (Bai et al., 2023; Adekoya et al., 2022; Elsayed et al., 2024; Abdullah et al., 2023).

The dynamic weights for the portfolio based on the MCP strategy Eq. (16) are presented in the LHS of Fig. 9. Hedge assets according to the MCP strategy are assets that pose minimum volatility integration risks. Gold futures receive exacerbated volatility transmissions from SPX and oil futures especially after 2005. Consequently, the MCP strategy is more conservative to gold during the GFC, ESDC and COVID crises. Crude and heating oil futures are also consistently weighted lower in the portfolio during crises owing to their significant integration with each other and the SPX, particularly during AFC and GFC. During the ESDC, heating oil futures are weighted more heavily than crude oil futures. In contrast, crude oil futures are weighted more heavily during the oil price crash than heating oil futures. Our findings substantiate the hedge asset potential of natural gas futures in the portfolio. With minimal interactions with SPX, crude, and heating oil futures, they are heavily weighted during crises, maximising returns by minimising inter-future volatility spillovers. Similarly, lumber and corn futures are weighted higher during crises due to their limited volatility interaction with the rest of the portfolio. Copper futures significantly interact with oil futures during the GFC and ESDC and are subsequently weighted less during those crises. Despite SPX being a constant volatility contagion source, the only instance where SPX is weighted to zero is at the onset of the DBC. During the COVID-19 pandemic, crude oil and heating oil futures are weighted at zero coinciding with their exacerbated volatility spillover conditions. Overall, the MCP strategy places greater emphasis on SPX, natural gas, lumber, silver, and corn futures.

The MVP strategy minimises portfolio risk by reducing conditional covariances between assets within the portfolio (Markowitz, 1959). The dynamic weights for the portfolio based on the MCP strategy are presented in the RHS of Fig. 9. Both the MCP and MVP strategies require estimating the time-varying variance–covariance matrix of the TVP-VAR-SV model Eq. (7). Additionally, the MCP weights require the computation of the generalised FEVDs to compute the pairwise connectedness indices. Our results indicate that the MVP strategy places heavier emphasis on gold futures during crisis periods and on SPX during non-crisis periods. Interestingly, the MVP strategy weighs lumber more than gold during the GFC. We observe the typical MVP characteristic of portfolio concentration (Maillard et al., 2010; Clarke et al., 2011), with minimal weights assigned to silver, crude oil, heating oil, and wheat futures.

Table 4
Descriptive Statistics — Cumulative returns of the portfolio.

	MCP	MVP	EWP
Mean	3.11	1.97	2.97
Min	−0.0	−0.03	−0.0
Max	13.35	10.67	7.22
Standard deviation	2.64	2.07	2.3

Fig. 10 plots the historical evolution of cumulative portfolio returns under the MCP, MVP, and EWP strategies. Our results indicate that the MCP strategy consistently outperforms the highly concentrated MVP strategy during crises and also surpasses the EWP strategy during the pandemic-induced crisis.

Table 4 depicts the descriptive statistics for the cumulative portfolio returns of the three strategies. The MCP strategy generally yields higher average returns, while the MVP strategy exhibits the lowest return volatility.

Hedge Effectiveness (HE) (Ederington, 1979) measures the diversification potential of the hedged portfolio over the unhedged individual asset. It is calculated as:

$$HE = 1 - \frac{var(R_{portfolio})}{var(R_{asset})} \tag{20}$$

where $var(R_{portfolio})$ is the variance of the return of the different strategies and $var(R_{asset})$ is the variance of the individual asset (future or SPX). A HE value close to 1 indicates a better risk diversification potential for the portfolio compared to the individual asset. Table 5 depicts the mean weight of the portfolio along with the hedge effectiveness of individuals asset for the different portfolio construction strategies (MCP, MVP and EWP). We find that the HE is smaller and at times negative for the MCP and EWP portfolios, whereas the values are closer to unity for the MVP portfolio. This is consistent as the MVP portfolio by definition minimises the variance of the portfolio returns; thereby minimising risk. However, this does not imply profitability. The MCP strategy ensures greater cumulative returns by placing more emphasis on SPX, lumber natural gas, silver and agricultural futures.

6. Conclusion

Our study investigates the impacts of time-varying volatility spillovers across major commodity futures (gold, silver, crude oil, heating oil, natural gas, lumber, copper, wheat and corn) and SPX from January 1990 to February 2022. We highlight the dynamic nature of the transmission effects across precious metals, industrial goods, energy and agricultural futures. Incorporating SPX in the analysis accounts for spillover effects due to exposure to common shocks fuelled by the increasing speculative participation in futures markets. The extended timeline covers key crises, including the AFC, GFC, ESDC, the oil price crash and COVID-19 pandemic-induced crisis.

We employ the TVP-VAR-SV model (Primiceri, 2005; Cogley and Sargent, 2005; Nakajima, 2011) to estimate time-varying contemporaneous and lagged effects, as well as the impact of exogenous shocks. The model parameters follow a random walk specification, estimated via Bayesian MCMC techniques. The TVP-VAR framework effectively captures the dynamic interdependencies between variables, allowing for the analysis of both mutual influences and the transmission of shocks. Additionally, the SV component (Black, 1976) addresses variability in exogenous shocks. Volatility spillover indices are computed using the generalised FEVD-based DY-spillover index (Diebold and Yilmaz, 2008, 2012; Diebold and Yılmaz, 2014).

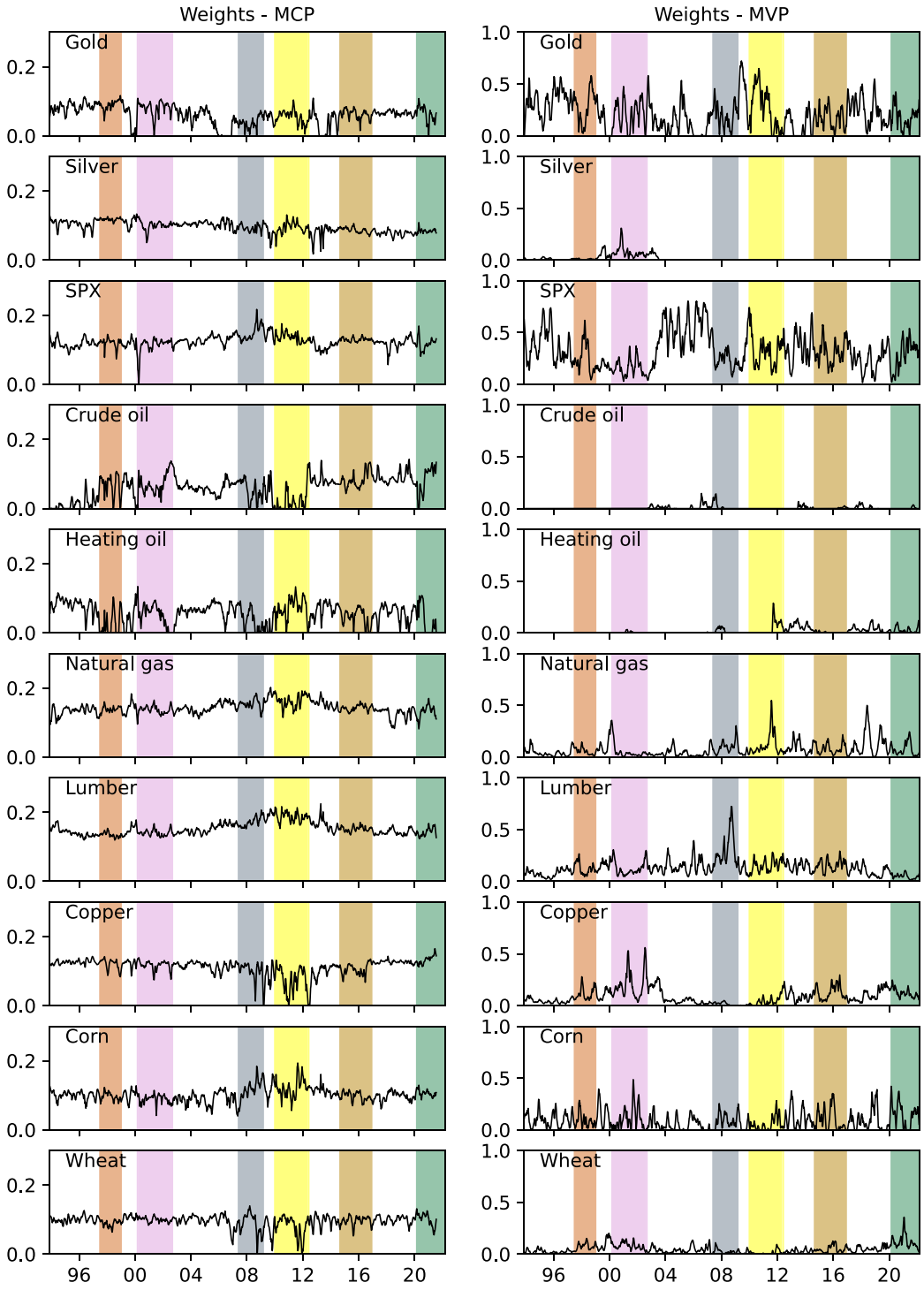

Fig. 9. Time-varying Multivariate Portfolio Weights
The LHS of the Figure plots the dynamic weights following the MCP strategy (see Eq. (16)) computed from the Pairwise Connectedness Indices (see Eq. (15)) computed from the TVP-VAR-SV model. The RHS of the Figure plots the dynamic weights following the MVP strategy (see Eq. (17)) computed from the Variance-Covariance matrices of the TVP-VAR-SV model. The various crisis periods are shaded as reported in Table 2.

Our results indicate that SPX is the largest net transmitter of volatility information. Significant volatility spillovers from SPX to energy futures exist that exacerbate during crises, alluding to the *financialisation* of energy futures. In addition, gold futures receive heightened volatility transmissions during crises, alluding to the *flight to quality* characteristic exhibited by investors. Natural gas futures do not have significant within-sector transmissions with crude and heating oil futures, supporting the theory that natural gas prices have decoupled from prices of other oil futures. Additionally, the degree of integration of natural gas futures with SPX is significantly lower than other energy futures, suggesting potential viability as a hedge asset. Agricultural futures primarily exhibit a high degree of within-sector volatility interconnectedness and could also serve as viable hedge assets during crises. A unique finding from the COVID-19 crisis and the consequent supply chain disruptions indicate heightened volatility transmissions from lumber to natural gas futures, which was unseen in previous

Table 5
Mean portfolio weights and Hedge Effectiveness.

	MCP		MVP		EWP	
Asset class	Mean Weight	HE	Mean Weight	HE	Mean Weight	HE
Gold	.06	0.04	.21	0.55	.10	−0.11
Silver	.10	0.71	.01	0.86	.10	0.66
SPX	.12	0.24	.32	0.64	.10	0.12
Crude oil	.06	0.95	.01	0.98	.10	0.94
Heating oil	.06	0.8	.02	0.91	.10	0.77
Natural gas	.14	0.91	.07	0.96	.10	0.9
Lumber	.15	0.83	.13	0.92	.10	0.81
Copper	.11	0.6	.09	0.81	.10	0.53
Corn	.10	0.68	.09	0.85	.10	0.64
Wheat	.10	0.71	.05	0.86	.10	0.67
Average	.10	0.647	.10	0.834	.10	0.593

This table reports the averaged portfolio weights and Hedge Effectiveness Eq. (20) of the overall portfolio under the MCP, MVP and EWP strategies. A higher HE value indicates a larger risk reduction and vice versa.

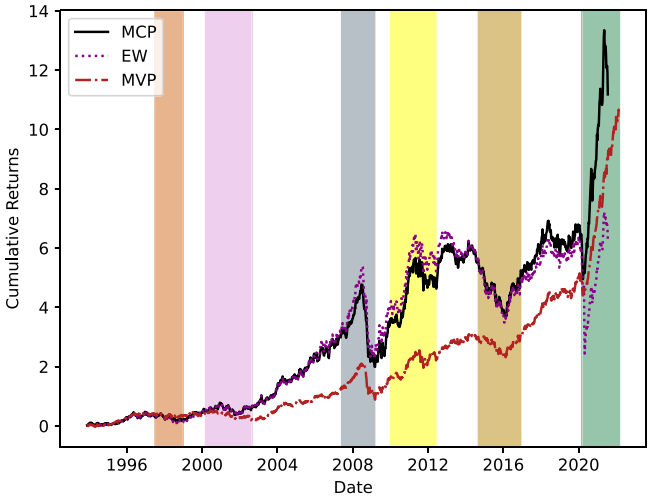

Fig. 10. Weighted Portfolio Performance
Cumulative portfolio returns under the MCP and MVP and EWP strategies. The various crisis periods are shaded as reported in Table 2.

crises.

Analysing the propagation of volatility transmissions is integral for policymakers and investors to gauge the aftermath of high volatility events on specific asset and the downstream impacts on related assets. Policymakers benefit by identifying key volatility transmitters and receivers. Volatility transmitting assets pose a risk of exacerbating contagion effects throughout the economy. By pinpointing these sources and understanding the channels of risk propagation, policymakers can implement more effective regulatory measures to mitigate systemic risks. For fund managers, identifying key volatility transmitters and receivers within their portfolios can provide a strategic advantage. Our spillover analyses reveal that the financialisation of energy futures — particularly crude and heating oil futures, lead to exacerbated volatility in these assets during economic and financial crises, as stock market shocks spill over into energy markets. However, demand and supply shocks in the oil market do not significantly affect SPX volatility.[23] While, conventional hedging assets like gold futures experience increased volatility from SPX and oil futures during crises, making them less effective, natural gas futures show minimal interaction with SPX and other energy futures, maintaining stability. We substantiate our recommendations by constructing dynamic MCP weights (Broadstock et al., 2020) (See Fig. 9), which indicate that less interconnected assets, such as natural gas, lumber, and agricultural futures, offer effective hedging opportunities, making them valuable additions to a diversified portfolio during periods of crises. Additionally, identifying inter-asset volatility linkages contain significant information that could potentially enhance fund managers' ability to predict future asset volatility more accurately.

[23] The brief period in April 2020, when oil futures traded at negative prices and transitioned to net volatility transmitter to SPX being an exception.

CRediT authorship contribution statement

Shietal Ramesh: Writing – original draft, Visualization, Validation, Software, Methodology, Investigation, Formal analysis, Data curation, Conceptualization, Writing – review & editing. **Rand Kwong Yew Low:** Writing – review & editing, Validation, Supervision, Conceptualization. **Robert Faff:** Writing – review & editing.

Declaration of competing interest

The authors declare that they have no known competing financial interests or personal relationships that could have appeared to influence the work reported in this paper.

Acknowledgements

This research was supported by an Australian Government Research Training Program Scholarship.

This research was supported by the use of the ARDC Nectar Research Cloud, a collaborative Australian research platform supported by the NCRIS-funded Australian Research Data Commons (ARDC).

We want to thank Leah South and Matt Sutton from the Queensland University of Technology for their help.

This paper was presented at the 2023 Conference on Asia-Pacific Financial Markets (CAFM) and the 2024 Accounting & Finance Association of Australia and New Zealand (AFAANZ) Doctoral Symposium. The comments of participants at the event are gratefully acknowledged.

Appendix A. Data - crisis timelines and event-based statistical analysis

A.1. Crisis timelines

Our study's timeline spans three decades, from January 1990 to February 2022. This period encompasses significant economic crises, commodity price crashes, and a crisis induced by a pandemic. We detail the justification for the beginning and end of the various crises, along with the relevant sources here.

1. **Asian Financial Crisis (AFC) (July 1997–December 1998):** The crisis began in July 1997 with the devaluation of the Thai Baht, sparking widespread capital outflows across Asia. It lasted until December 1998, concluding with the implementation of IMF-led stabilisation programs, as detailed by Kaminsky and Schmukler (1999), Lien et al. (2018) and Krugman (2000).
2. **Dot-com Bubble Crash (DBC) (March 2000–October 2002):** After nearly peaking at 5048 points on March 10, 2000, NASDAQ began to sharply decline, as major companies started placing large sell orders on their stocks. This triggered a panic among investors, causing the stock market to lose over 10% of its value within weeks. NASDAQ continued to fall, reaching 1,139 by October 2002, signalling the end of the dot-com bubble (Timeline retrieved from the Federal Reserve Bank of St. Louis.).
3. **Global Financial Crisis (GFC) (June 2007–February 2009):** The crisis began in July 2007 when Standard and Poor's and Moody's Investor Services downgraded over 100 bonds backed by second-lien subprime mortgages. Additionally, Bear Stearns informed investors that it would suspend redemptions from its High-Grade Structured Credit Strategies Enhanced Leverage Fund, subsequently liquidating two hedge funds invested in various types of mortgage-backed securities. The crisis came to an end in February 2009 with the implementation of the U.S. government's economic stimulus package, as documented by the Federal Reserve Bank of St. Louis.
4. **European Sovereign Debt Crisis (ESDC) (January 2010–May 2012):** The crisis began in January 2010 when rising sovereign debt levels compelled lenders to demand higher interest rates from Eurozone countries grappling with significant debt and deficit issues. Greece, Portugal, and Ireland faced substantial downgrades to junk status by international credit rating agencies, intensifying investor anxieties. The crisis ended in May 2012, following the European Union's financial assistance and the implementation of crucial reforms, as highlighted by Ehrmann and Fratzscher (2017) and Arellano et al. (2012)
5. **Oil price crash (September 2014–November 2016):** The crsis began in September 2014, driven by a sharp decline in oil prices from a peak of $100 in June 2014. This decline was further compounded by OPEC's decision not to cut production levels despite falling prices, as they aimed to maintain market share and pressure higher-cost producers, particularly U.S. shale producers. The crisis ended in November 2016, when OPEC agreed to cut production for the first time in eight years, with participation from non-OPEC producers, as reported by Fantazzini (2016).
6. **COVID-19 pandemic-induced crisis (March 2020–February 2022):** The crisis began in March 2020 when the World Health Organisation declared the Novel Coronavirus outbreak a pandemic, marking a significant period of global economic disruption and uncertainty, which continued until February 2020, which is also the endpoint of our data scope (Timeline retrieved from the Federal Reserve Bank of St. Louis).

A.2. Crisis-specific descriptive statistics

Tables A.6–A.16 present the period-wise descriptive statistics to emphasise changes in key characteristics during crises.

Appendix B. MCMC sampling methodology to estimate coefficients in TVP-VAR-SV model

The model introduced in Section 3.1 has several time-varying parameters that require estimation: $\mathbf{A}_t$, $\mathbf{B}_{m,t}$ and $\boldsymbol{\Sigma}_t$. This section outlines the MCMC algorithm used in this study.

B.1. Prior estimation

Priors refer to the probability distributions that express our beliefs or assumptions about the data before undertaking any data analysis. The first 200 observations (from Jan 1, 1990, to Oct 1993) are chosen to calibrate our prior distributions. Robust priors are necessary to avoid implausible behaviours from the time-varying parameters. We follow Primiceri (2005) and Nakajima (2011) and set up tighter priors for the time-varying coefficient $\boldsymbol{\beta}_t$ and more diffuse priors for the time-varying simultaneous relations $\boldsymbol{\alpha}_t$ and the time-varying SV component h_t. We estimate the initial conditions using a conventional OLS approach where we solve the following SVAR model :

$$\mathbf{y}_t = \mathbf{X}_t'\beta + \xi_t, \tag{B.1}$$

where β is the constant to be estimated, while $[\Xi]_{n\times n}$ from $\xi_t \sim N(0, \Xi)$ is estimated via the sum-squared error of the constant VAR. The estimations are found via standard OLS equations (Greene, 2022; Lütkepohl, 2005):

$$\hat{\beta}_{OLS} = E(\hat{\beta}) = \left(\sum_{t=1}^{T}(\mathbf{X}_t\mathbf{X}_t')\right)^{-1}\left(\sum_{t=1}^{T}\mathbf{X}_t\mathbf{y}_t\right) \tag{B.2}$$

$$\hat{\Xi} = \frac{1}{T-k}\sum_{t=1}^{T}(\mathbf{y}_t - \mathbf{X}_t'\hat{\beta}_{OLS})(\mathbf{y}_t - \mathbf{X}_t'\hat{\beta}_{OLS})' \tag{B.3}$$

$$V(\hat{\beta}_{OLS}) = \left(\sum_{t=1}^{T}\mathbf{X}_t\hat{\Xi}^{-1}\mathbf{X}_t'\right)^{-1}. \tag{B.4}$$

To get the estimates for the terms in $\mathbf{A}^{-1}\boldsymbol{\Sigma}$, we need to perform a Cholesky decomposition, or more specifically an LDL decomposition, on $\hat{\Xi} = \hat{\mathbf{A}}_{OLS}^{-1}\hat{\Sigma}_0\hat{\Sigma}_0'(\hat{\mathbf{A}}_{OLS}^{-1})'$ to get:

$$\hat{\Xi} = \mathbf{L}\mathbf{D}\mathbf{L}', \tag{B.5}$$

$$\hat{\mathbf{A}}_{OLS} = \mathbf{L}^{-1} \tag{B.6}$$

$$\hat{\boldsymbol{\Sigma}}_{OLS} = \sqrt{\mathbf{D}}, \tag{B.7}$$

where $\mathbf{L}$ is a lower-triangular matrix and $\mathbf{D}$ is a diagonal matrix.

To estimate the variance of $\boldsymbol{\alpha}_t$, we observe the distribution of possible covariance matrices for Ξ by drawing 10000 samples from the appropriate Inverse Wishart distribution with T degrees of freedom and $\hat{\Xi}$ as the scale matrix. For each sampled draw, we calculate the associated $\boldsymbol{\alpha}_t$ via the LDL decomposition as shown above. Now that we have 10000 different possible $\boldsymbol{\alpha}_t$ vectors, we take the variance in these vectors to get the prior for $Var(\hat{\mathbf{A}}_{OLS})$.

Summarising, the priors of the state variables and the corresponding hyperparameters are given as follows:

$$\beta_0 \sim N(\hat{\beta}_{OLS}, 4 * V(\hat{\beta}_{OLS})), \tag{B.8}$$

$$A_0 \sim N(\hat{A}_{OLS}, 4 * V(\hat{A}_{OLS})), \tag{B.9}$$

$$\log\sigma_0 \sim N(\log\sigma_{OLS}, I_n), \tag{B.10}$$

$$Q \sim IW(k_Q^2 * 200 * I_n, 200), \tag{B.11}$$

$$S_1 \sim IW(k_S^2 * 2 * V(\hat{A}_{1,OLS}), 2), \tag{B.12}$$

$$S_2 \sim IW(k_S^2 * 3 * V(\hat{A}_{1,OLS}), 3), \tag{B.13}$$

$$W \sim IW(k_W^2 * 4 * I_n, 4) \tag{B.14}$$

We empirically set the following values $k_Q = 0.00001$, $k_S = 0.1$, $k_W = 1$ to represent diffuse (i.e., uninformative) priors for the hyperparameters. The selected hyper-parameters yield stationary solutions over every draw of β_t generated using the MCMC sampling algorithm. The stationarity condition is an essential condition to ensure robustness of the MCMC sampling draws. If the MCMC process fails to produce stationary solutions, the iteration is rejected, and the algorithm reverts to the previously accepted β_t value to compute the values for α_t and Σ_t. A high rejection rate would indicate that the posterior means of β_t are

Table A.6
Descriptive Statistics: AFC (Jul 1997–Dec 1998).

Asset class	Mean	Median	Min	Max	Skew	Kurtosis	Jarque–Bera Test
Gold	5.45	4.86	1.08	16.52	1.06	2.62	37.03***
Silver	12.07	11.63	1.42	31.35	0.68	0.62	7.34**
SPX	8.11	7.13	3.26	28.83	2.54	7.84	283.48***
Crude oil	13.73	12.31	2.58	43.57	1.67	3.94	86.99***
Heating oil	12.17	11.03	3.33	35.65	1.79	4.14	97.17***
Natural gas	19.89	18.31	7.68	40.91	0.68	−0.0	6.05*
Lumber	10.99	11.11	2.91	19.45	0.07	−0.25	0.27
Copper	9.89	9.46	1.5	21.29	0.65	0.35	5.88*
Corn	9.03	8.48	0.64	21.29	0.69	0.07	6.2*
Wheat	8.91	8.6	3.14	20.16	1.31	3.76	68.43***

The Jarque–Bera test is for the following significance levels: *** indicates significance at 1% level, ** indicates significance at 5% level and * indicates significance at 10% level.

Table A.7
Descriptive Statistics: Pre-DBC (Jan 1999–Feb 2000).

Asset class	Mean	Median	Min	Max	Skew	Kurtosis	Jarque–Bera Test
Gold	6.25	4.18	1.12	34.66	2.89	10.39	365.13***
Silver	9.12	8.17	2.57	26.56	1.36	2.61	36.78***
SPX	8.02	8.08	1.7	15.6	0.14	−0.49	0.83
Crude oil	14.38	13.98	4.19	37.48	1.17	3.18	40.25***
Heating oil	14.22	13.44	3.14	33.88	0.83	1.45	12.45***
Natural gas	17.54	16.86	7.25	36.68	0.61	0.19	3.95
Lumber	9.78	9.35	3.52	19.26	0.47	−0.38	2.66
Copper	9.87	9.31	3.0	23.68	0.72	0.6	6.28*
Corn	8.46	7.7	2.34	21.26	1.2	1.17	18.43***
Wheat	9.97	9.26	2.45	26.34	1.14	2.86	34.49***

The Jarque–Bera test is for the following significance levels: *** indicates significance at 1% level, ** indicates significance at 5% level and * indicates significance at 10% level.

Table A.8
Descriptive Statistics: DBC (Mar 2000–Oct 2002).

Asset class	Mean	Median	Min	Max	Skew	Kurtosis	Jarque–Bera Test
Gold	5.33	4.81	0.93	21.6	2.14	8.37	507.51***
Silver	6.3	5.67	1.41	25.79	1.92	7.92	444.91***
SPX	9.59	8.43	2.48	23.45	1.06	0.52	27.27***
Crude oil	15.18	14.22	0.71	55.17	2.16	9.3	604.12***
Heating oil	14.93	14.16	2.43	48.01	1.28	4.06	132.21***
Natural gas	23.75	22.56	6.66	69.05	1.13	2.06	53.9***
Lumber	13.0	12.55	4.53	21.52	0.21	−0.93	5.95*
Copper	7.59	7.11	1.13	20.86	1.08	2.3	57.22***
Corn	8.71	7.85	1.79	24.95	1.24	1.91	56.43***
Wheat	9.76	9.5	2.25	28.95	1.19	3.66	109.77***

The Jarque–Bera test is for the following significance levels: *** indicates significance at 1% level, ** indicates significance at 5% level and * indicates significance at 10% level.

Table A.9
Descriptive Statistics: Pre-GFC (Nov 2002–May 2007).

Asset class	Mean	Median	Min	Max	Skew	Kurtosis	Jarque–Bera Test
Gold	7.1	6.59	1.46	25.3	1.56	4.51	299.36***
Silver	11.89	10.2	2.26	54.21	2.44	8.72	994.77***
SPX	5.24	4.62	1.56	14.15	1.21	1.51	81.58***
Crude oil	13.31	12.53	3.1	34.27	1.07	2.34	99.89***
Heating oil	14.65	13.59	4.34	36.21	1.21	2.35	113.48***
Natural gas	20.32	18.98	5.16	89.13	1.91	8.36	841.44***
Lumber	11.69	11.69	2.44	21.28	−0.05	−0.17	0.39
Copper	11.57	10.07	3.5	44.24	1.74	4.59	330.15***
Corn	10.01	9.22	2.16	36.7	1.28	3.02	156.29***
Wheat	11.72	10.93	2.89	30.17	1.14	2.14	97.95***

The Jarque–Bera test is for the following significance levels: *** indicates significance at 1% level, ** indicates significance at 5% level and * indicates significance at 10% level.

based on limited variation, potentially misrepresenting the underlying data-generating process.

Using the current set of priors for the parameters and the hyper-parameters, we do not reject a single iteration of the 20000 MCMC sampling iterations. This implies that our empirically tested values for k_Q, k_S and k_W will lead to posterior estimates that are stationary and will aid the MCMC process to model the underlying data process effectively. Additionally, we plot the convergence of the estimated posterior distributions of the model parameters using a Cauchy convergence test (see Fig. C.13). With our priors, the MCMC model achieves convergence

Table A.10
Descriptive Statistics: GFC (Jun 2007–Feb 2009).

Asset class	Mean	Median	Min	Max	Skew	Kurtosis	Jarque–Bera Test
Gold	10.7	9.47	4.16	36.11	1.57	4.19	103.97***
Silver	16.9	14.12	4.86	51.85	1.38	1.56	37.89***
SPX	12.87	10.51	2.91	48.67	1.8	2.84	79.66***
Crude oil	19.0	15.34	5.42	49.66	1.11	0.19	18.91***
Heating oil	16.38	14.39	4.66	40.0	1.09	0.53	19.11***
Natural gas	18.66	17.58	6.02	47.76	0.97	1.4	21.59***
Lumber	12.69	12.08	4.27	34.67	1.1	1.88	31.7***
Copper	17.05	14.41	5.31	55.85	1.56	2.39	58.5***
Corn	15.85	14.24	3.64	36.68	0.91	0.44	13.42***
Wheat	18.58	16.52	7.21	54.88	1.62	3.69	91.32***

The Jarque–Bera test is for the following significance levels: *** indicates significance at 1% level, ** indicates significance at 5% level and * indicates significance at 10% level.

Table A.11
Descriptive Statistics: Pre-ESDC (Mar 2009–Dec 2009).

Asset class	Mean	Median	Min	Max	Skew	Kurtosis	Jarque–Bera Test
Gold	8.03	7.28	3.31	26.5	2.49	9.22	201.22***
Silver	14.91	13.51	5.97	46.27	2.67	11.25	284.31***
SPX	9.84	8.32	1.35	25.28	1.07	0.85	9.76**
Crude oil	17.24	14.57	3.44	44.81	1.56	2.58	30.06***
Heating oil	16.71	14.81	6.83	40.52	1.33	1.68	18.08***
Natural gas	25.29	23.03	10.43	44.76	0.64	−0.59	3.66
Lumber	15.83	15.65	2.73	27.71	−0.07	−0.6	0.7
Copper	15.48	15.35	3.85	27.78	0.2	−0.26	0.4
Corn	14.69	14.05	6.03	32.37	0.78	0.31	4.68
Wheat	15.5	15.2	7.29	33.83	0.72	0.5	4.23

The Jarque–Bera test is for the following significance levels: *** indicates significance at 1% level, ** indicates significance at 5% level and * indicates significance at 10% level.

Table A.12
Descriptive Statistics: ESDC (Jan 2010–May 2012).

Asset class	Mean	Median	Min	Max	Skew	Kurtosis	Jarque–Bera Test
Gold	7.49	6.96	2.06	24.38	1.67	4.2	150.9***
Silver	15.63	14.27	2.57	72.55	2.94	15.2	1394.61***
SPX	7.61	6.6	0.67	33.85	1.83	6.7	306.33***
Crude oil	11.98	10.94	3.2	31.34	1.14	1.29	35.86***
Heating oil	10.29	10.05	2.25	28.86	0.96	1.83	37.01***
Natural gas	16.26	15.03	5.89	37.09	1.0	1.24	28.96***
Lumber	14.71	14.76	4.08	29.25	0.12	−0.02	0.3
Copper	11.69	10.68	3.35	34.44	1.57	3.75	125.75***
Corn	13.08	11.57	3.98	41.95	1.48	3.14	97.83***
Wheat	15.38	13.95	2.69	44.95	1.19	2.17	54.41***

The Jarque–Bera test is for the following significance levels: *** indicates significance at 1% level, ** indicates significance at 5% level and * indicates significance at 10% level.

Table A.13
Descriptive Statistics: Pre-OC (Jun 2012–Aug 2014).

Asset class	Mean	Median	Min	Max	Skew	Kurtosis	Jarque–Bera Test
Gold	6.99	6.29	0.63	32.34	2.55	11.61	783.12***
Silver	11.18	9.74	2.36	39.23	1.44	3.44	98.26***
SPX	4.75	4.33	0.71	11.05	0.78	0.09	11.87***
Crude oil	8.04	7.2	1.01	30.91	2.05	7.05	324.13***
Heating oil	6.85	6.36	1.89	21.35	1.28	3.13	79.66***
Natural gas	14.98	13.36	4.99	51.44	2.39	8.94	500.82***
Lumber	9.62	9.67	2.34	27.63	0.92	3.61	79.85***
Copper	7.29	6.95	2.46	24.62	1.42	4.15	123.13***
Corn	9.92	8.7	2.43	26.25	1.22	1.01	33.8***
Wheat	10.2	9.32	1.86	24.51	0.77	0.38	12.21***

The Jarque–Bera test is for the following significance levels: *** indicates significance at 1% level, ** indicates significance at 5% level and * indicates significance at 10% level.

to steady-state values after 20,000 iterations.

B.2. Sampling $\beta_t s$

The first stage of the Carter-Kohn algorithm is a Kalman filter. A Kalman filter assumes that the observed data is subject to measurement errors. This implies that the true data process is still unobservable. The Kalman Filter algorithm filters the measurement noise in order to learn more about the true data generating process (Kalman, 1960; Burmeister et al., 1986). The observed data (measurement equation) is given by:

$$\mathbf{y}_t = \mathbf{X}_t'\boldsymbol{\beta}_t + \boldsymbol{\xi}_t \tag{B.15}$$

where $\boldsymbol{\xi}_t$ is the measurement noise with $E(\boldsymbol{\xi}_t\boldsymbol{\xi}_t') = \mathbf{R}_t$. The unobservable process known as the state or transition equation is given by:

$$\boldsymbol{\beta}_t = \boldsymbol{\beta}_{t-1} + \mathbf{u}_t \tag{B.16}$$

Table A.14
Descriptive Statistics: Oil crash (Sep 2014–Nov 2016).

Asset class	Mean	Median	Min	Max	Skew	Kurtosis	Jarque–Bera Test
Gold	6.41	6.04	1.59	18.02	1.24	2.67	65.22***
Silver	10.92	10.18	2.68	26.38	0.71	−0.05	9.87**
SPX	5.64	5.18	0.66	20.0	1.14	2.24	50.18***
Crude oil	18.18	17.54	4.06	42.62	0.94	0.93	21.56***
Heating oil	15.22	13.99	3.73	39.17	0.99	1.16	26.03***
Natural gas	17.33	16.4	4.42	41.63	1.05	1.85	38.54***
Lumber	10.32	10.1	1.83	21.39	0.21	−0.36	1.49
Copper	8.77	8.29	1.17	22.53	1.01	1.81	36.15***
Corn	9.5	8.41	2.2	25.94	1.15	1.66	39.46***
Wheat	11.37	10.99	2.37	26.49	0.86	1.16	21.02

The Jarque–Bera test is for the following significance levels: *** indicates significance at 1% level, ** indicates significance at 5% level and * indicates significance at 10% level.

Table A.15
Descriptive Statistics: Pre-COVID (Dec 2016–Feb 2020).

Asset class	Mean	Median	Min	Max	Skew	Kurtosis	Jarque–Bera Test
Gold	4.57	4.23	1.18	17.02	1.89	7.19	464.09***
Silver	7.66	7.15	1.28	28.45	1.95	6.38	393.74***
SPX	4.85	3.71	0.98	20.98	2.13	5.41	333.28***
Crude oil	11.94	10.59	2.55	47.6	2.29	8.38	642.65***
Heating oil	9.85	9.39	2.28	36.6	1.71	6.43	373.52***
Natural gas	15.27	13.09	5.52	88.98	3.54	21.81	3703.9***
Lumber	11.98	10.73	1.45	30.23	0.82	0.44	20.31***
Copper	7.65	7.18	2.47	17.7	0.84	0.37	20.94***
Corn	7.78	6.71	1.74	28.41	1.61	3.93	181.78***
Wheat	10.73	9.67	3.79	26.69	0.93	0.35	25.48***

The Jarque–Bera test is for the following significance levels: *** indicates significance at 1% level, ** indicates significance at 5% level and * indicates significance at 10% level.

Table A.16
Descriptive Statistics: COVID (Mar 2020–Feb 2022).

Asset class	Mean	Median	Min	Max	Skew	Kurtosis	Jarque–Bera Test
Gold	7.07	6.4	1.44	26.88	1.75	4.49	140.27***
Silver	14.9	12.39	2.74	51.06	1.75	3.28	99.41***
SPX	8.54	6.21	1.41	54.87	3.57	14.98	1192.52***
Crude oil	21.23	13.3	4.8	211.04	4.62	24.47	2963.04***
Heating oil	15.49	11.98	3.43	66.42	2.39	6.6	287.71***
Natural gas	22.33	20.22	4.27	52.19	0.67	−0.24	8.04**
Lumber	22.52	21.23	5.33	50.13	0.71	0.61	10.44**
Copper	10.07	9.17	2.01	28.1	0.99	1.65	28.7***
Corn	10.54	9.44	2.18	27.76	1.35	1.65	43.6***
Wheat	11.95	11.16	4.23	41.52	2.36	12.16	736.65***

The Jarque–Bera test is for the following significance levels: *** indicates significance at 1% level, ** indicates significance at 5% level and * indicates significance at 10% level.

where $\mathbf{u}_t$ is the structural shock with $E(\mathbf{u}_t\mathbf{u}_t') = [\mathbf{Q}]_{(n(kn+1))\times(n(kn+1))}$. Note that we have no coefficient in front of β_{t-1} as we have packed the matrices such that β_t follows a random walk. We define $\beta_{t|s}$ as the conditional expectation $E(\beta_t|\beta_1,\dots,\beta_s)$ and the conditional variance $V_{t|s} = \text{Var}(\beta_t|\beta_1,\dots,\beta_s)$.

From the Kalman filter algorithm we get:

$$\beta_{t|t-1} = \beta_{t-1|t-1} \tag{B.17}$$

$$V_{t|t-1} = V_{t-1|t-1} + \mathbf{Q} \tag{B.18}$$

$$F_{t|t-1} = y_t - X_t'\beta_{t|t-1} \tag{B.19}$$

$$K_t = V_{t|t-1}X_t(X_t'V_{t|t-1}X_t + \mathbf{R}_t)^{-1} \tag{B.20}$$

$$\beta_{t|t} = \beta_{t|t-1} + K_tF_{t|t-1} \tag{B.21}$$

$$V_{t|t} = V_{t|t-1} - K_tX_t'V_{t|t-1}, \tag{B.22}$$

Eqs. (B.17) and (B.18) predict the one period ahead value of the state variable and its variance using only the parameters from the transition equation. The observed data y_t is not used up to this point. Eq. (B.19) calculates the conditional forecast error of the state variable β_t. We set the initial values (the priors) as: $\beta_{0|0} = \hat{\beta}_{OLS}$ and $V_{0|0} = 4V(\hat{\beta}_{OLS})$. Note that $y_t - X_t'\beta_{t|t-1}$ is the error in forecasting y_t given all its previous values. Upon calculating all the values for $\beta_{t|t}$ and $V_{t|t}$, we can better estimate the values of β_t and its variance by applying backward recursion (which effectively better smooths the data). Here the values of β_t and its variance calculated at every time point are used as the mean and variance of a Normal distribution of the potential future value; by randomly sampling from such a distribution, we can estimate the previous points starting from $t = T$:

$$\beta_{t|t+1} = \beta_{t|t} + V_{t|t}V_{t+1|t}^{-1}(\beta_{t+1} - \beta_{t|t}) \tag{B.23}$$

$$V_{t|t+1} = V_{t|t} - V_{t|t}V_{t+1|t}^{-1}V_{t|t}. \tag{B.24}$$

Here β_{t+1} is drawn randomly from a Normal distribution $N(\beta_{t|t}, V_{t|t})$ where $\beta_{t|t}$ and $V_{t|t}$ are taken from the calculated values during the Kalman filter step. Similarly, $V_{t+1|t} = V_{t|t} + \mathbf{Q}$. The result is that we now have a smoothed estimates: $\beta_{t|t+1}$ and $V_{t|t+1}$. Now we finally use these means and variances to get the values of β_t by randomly drawing from a Normal distribution: $N(\beta_{t|t+1}, V_{t|t+1})$.

B.3. Sampling α_ts

In order to model the contemporaneous relations amongst the model variables, we will draw the covariance states from Eq. (5).

$$\mathbf{A}_t(y_t - X_t'\beta_t) = \mathbf{A}_t\hat{y}_t = \mathbf{\Sigma}_t\varepsilon_t \tag{B.25}$$

Re-writing Eq. (B.25) as follows:

$$(\mathbf{I}_n + \alpha_t)\hat{y}_t = \mathbf{\Sigma}_t \varepsilon_t \tag{B.26}$$

$$\hat{y}_t = -\alpha_t \hat{y}_t + \mathbf{\Sigma}_t \varepsilon_t \tag{B.27}$$

$$\hat{y}_t = \begin{pmatrix} 0 & 0 & 0 & 0 & \dots & 0 \\ \alpha_{21,t} & 0 & 0 & 0 & \dots & 0 \\ \alpha_{31,t} & \alpha_{32,t} & 0 & 0 & \dots & 0 \\ \vdots & \ddots & \ddots & \ddots & \ddots & 0 \\ \alpha_{n1,t} & \dots & \dots & \dots & \alpha_{nn-1,t} & 0 \end{pmatrix} \begin{pmatrix} -y_{1,t} \\ -y_{2,1} \\ -y_{3,t} \\ \vdots \\ -y_{n,t} \end{pmatrix} + \mathbf{\Sigma}_t \varepsilon_t \tag{B.28}$$

$$\hat{y}_t = \begin{pmatrix} 0 \\ -\alpha_{21,t} y_{1,t} \\ -[\alpha_{31,t} y_{1,t} + \alpha_{32,t} y_{2,t}] \\ -[\alpha_{n1,t} y_{1,t} + \dots + \alpha_{nn-1,t} y_{n-1,t}] \end{pmatrix} + \mathbf{\Sigma}_t \varepsilon_t \tag{B.29}$$

$$\hat{y}_t = \begin{pmatrix} 0 & 0 & \\ -\hat{y}_{1,t} & & \\ 0 & -\hat{y}_{[1,2],t} se & \\ 0 & 0 & -\hat{y}_{[1,2,\dots,n-1],t} \end{pmatrix}_{[n \times \frac{n(n-1)}{2}]} \begin{pmatrix} \alpha_{21,t} \\ \alpha_{31.t} \\ \alpha_{32.t} \\ \vdots \\ \alpha_{n1,1} \\ \vdots \\ \alpha_{nn-1,t} \end{pmatrix} + \mathbf{\Sigma}_t \varepsilon_t \tag{B.30}$$

$$\hat{y}_t = \mathbf{Z}_t \boldsymbol{\alpha}_t + \mathbf{\Sigma}_t \varepsilon_t \tag{B.31}$$

As observed in Eq. (B.31), the model though Gaussian has a nonlinear state form. The vector $[\hat{y}_t, \alpha_t]$ is not jointly normal as the dependent variable of the observation equation $\hat{y}_t$ appears on both sides of the equation. We can therefore not use Kalman filter based smoothers to compute the conditional distributions as we did for sampling the coefficient states β_t. As a workaround we write separate model equations for every row of the previous equation into $n-1$ equations where the ith equation is (Primiceri, 2005):

$$\hat{y}_{[1,\dots,i]t} = -\hat{y}_{[1,\dots,i]t} \alpha_{i,t} + \sigma_{i,t} \epsilon_{i,t} \tag{B.32}$$

where the vector of α_t-values $\alpha_{i,t} = [\alpha_{i1}, \dots, \alpha_{i,i-1}]$ is from the $i+1$ row of A_t. By partitioning into separate equations, the assumption is that the variance of the noise term in the random walk process is block diagonal:

$$\alpha_{i,t} = \alpha_{i,t-1} + \zeta_{i,t}, \tag{B.33}$$

where the matrices $[\mathbf{S}_i]_{i \times i}$ are the associated covariance matrices for the noise term $[\zeta_{i,t}]_{i,1}$. The block diagonal form ensures that we can implement the Kalman filter and recursion separately equation by equation. In this case, we have different state variables that belong to distinct and subsequent time periods. The dependent variable $\hat{y_{i,t}}$ no longer appears in the right hand side of the equation.

To draw the values of α_t, we apply a similar stream of logic to estimating β_t. We draw α_t by separately drawing each of the rows $\alpha_{i,t}$. The Kalman filter recursively computes the following:

$$\alpha_{i,t|t-1} = \alpha_{i,t-1|t-1} \tag{B.34}$$

$$V_{i,t|t-1} = V_{i,t-1|t-1} + \mathbf{S_i} \tag{B.35}$$

$$K_{i,t} = V_{i,t|t-1} Z_t' (Z_t V_{i,t|t-1} Z_t' + \exp h_{i,t}^2)^{-1} \tag{B.36}$$

$$\alpha_{i,t|t} = \alpha_{i,t|t-1} + K_{i,t}(y_t - Z_t \alpha_{i,t|t-1}) \tag{B.37}$$

$$V_{i,t|t} = V_{i,t|t-1} - K_{i,t} Z_t V_{i,t|t-1} \tag{B.38}$$

where the notation alludes to the way it was defined when drawing β_t. Similarly, the backward recursions are given by:

$$\alpha_{i,t|t-1} = \alpha_{i,t|t} + V_{i,t|t} V_{i,t+1|t}^{-1} (\alpha_{i,t+1} - \alpha_{t|t}) \tag{B.39}$$

$$V_{i,t|t+1} = V_{i,t|t} - V_{i,t|t} V_{i,t+1|t}^{-1} V_{i,t|t} \tag{B.40}$$

We now generate the posterior values of α_{it} by drawing from a Normal distribution: $N(\alpha_{i,t|i,t+1}, V_{i,t|i,t+1})$.

B.4. Sampling Σ_ts

We will now draw the volatility states in order to capture the impact of the time-varying exogenous shocks on the model system. Rewriting Eq. (5) as:

$$A_t(y_t - X_t' \beta_t) = y_t^* = \Sigma_t \varepsilon_t \tag{B.41}$$

This non-linear measurement equation can be converted into a linear form by squaring and taking logarithms of every element of Eq. (B.41). As $(y_{it}^*)^2$ is very small, following Fuller (1995), we introduce an offset constant c to ensure a more robust estimation process. The state space form for the volatility states are given by:

$$y_t^{**} = 2h_t + e_t \tag{B.42}$$

$$h_t = h_{t-1} + \eta_t \tag{B.43}$$

where:

$$y_{i,t}^{**} = \log[(y_{i,t}^*)^2 + \bar{c}] \tag{B.44}$$

$$\bar{c} = .001 \tag{B.45}$$

$$e_{i,t} = log(\epsilon_{i,t}^2) \tag{B.46}$$

$$h_{i,t} = \log \sigma_{i,t} \tag{B.47}$$

The transformed equations while linear are still non-Gaussian as the innovations in the measurement equation $e_{i,t}$ follows a $\ln \chi^2(1)$ process.[24] The algorithm by Carter and Kohn (1994) relies on Kalman filtering and smoothing to derive the process. This will necessitate that the distribution process along with the model errors follow a Gaussian process. As the variance–covariance matrix of e's is an identity matrix, the variance–covariance matrix of e's are also diagonal, therefore allowing the use of several independent mixture of normal approximation for e_t. That is, we now work component-wise across every dimension and find the best Gaussian that explains the current component of e_t.

Kim et al. (1998) in their paper develop an approximation for the $\ln \chi^2$ distribution using several mixture Gaussian models.

$$f(e_{i,t}) = \Sigma_{j=1}^{K} q_j f_N(e_{i,t} | m_j - 1.2704, v_j^2) \tag{B.48}$$

where the density function of the Gaussian distribution:

$$f_N(e_{i,t}) = \frac{1}{v_j \sqrt{2\pi}} \exp\left(-\frac{1}{2} \frac{(e_{i,t} - (m_j - 1.2704))^2}{v_j} \right) \tag{B.49}$$

Specifically they use seven normal densities with component probabilities q_j, mean $m_j - 1.2704$ and variances v_j^2 where $j = 1, 2, \dots, 7$ to approximate the density of the $\ln \chi^2(1)$ distribution. The values of q_j, m_j, v_j^2 indicating the implied weights, means and variances are given in Kim et al. (1998) where they found them via numerical optimisation.

The Carter Kohn algorithm however will only accommodate for one Gaussian error. As a workaround in dealing with the mixture Gaussian approximation of the error term from Eq. (B.48), like Primiceri (2005), we follow the approach taken by Kim et al. (1998) to select the most likely of the 7 Gaussians that explains the noise at a given point in time. We define an indicator variable $G_t = (G_{1,t}, \dots, G_{n,t})$ where $G_{j,t} \in \{1, \dots, 7\}$ where for a given time t, $G_{j,t}$ indicates the best Gaussian for component j of y_t^{**} (which we denote as $y_{j,t}^{**}$). We calculate $G_{j,t}$ by sampling the probability distribution:

$$P(G_{j,t} = i) = q_i f_N(y_{j,t}^{**} | 2h_{j,t} + m_i, v_i^2), \tag{B.50}$$

where $h_{j,t}$ denotes component j of h_t. In practice we simply take the cumulative distribution of $P(G_{j,t} = i)$ over all i and then using the resulting bins across i and then matching them against a uniformly sampled random number to draw the value of $G_{j,t}$. Once we have drawn all values of G_t, we can then use this indicator variable to select the

[24] The degree of freedom of the $\ln \chi^2$ is 1 as we iterate through each individual element in the model system.

appropriate Gaussian to get the mean and variance value for η_t to subsequently write down the equations for the Kalman filter:

Denote the best Gaussian for component j (which has a mean $m_{G_{j,t}}$ and variance $v_{G_{j,t}}$) of y_t^{**} (that is, $y_{j,t}^{**}$) as $M_{G_{j,t}} \sim N(m_{G_{j,t}}, v_{G_{j,t}})$. The measurement equation becomes $y_{j,t}^{**} = 2h_t + M_{G_{j,t}}$. However, we note that the mean of the noise term $M_{G_{j,t}}$ is not zero. Thus, we subtract its mean $m_{G_{j,t}}$ from both sides to obtain the new measurement and transition equations:

$$y_{j,t}^{***} = \tfrac{1}{2}(y_{j,t}^{**} - m_{G_{j,t}}) = h_{j,t} + e_{j,t}^{*} \tag{B.51}$$

$$h_{j,t} = h_{j,t-1} + \eta_{j,t} \tag{B.52}$$

where $e_{j,t}^{*} \sim N(0, v_{G_{j,t}}^2/4)$ in which we have additionally divided by 2 for convenience (scaling the variance appropriately). Note that $\eta_{j,t}$, the component j of η_t, can be treated individually as $\mathbf{W}$ is diagonal (that is, there is no covariance amongst the different components of the noise terms here). To apply the Carter-Kohn algorithm, we once again start with the accompanying Kalman filtering (only this time as component-wise scalars):

$$h_{j,t|j,t-1} = h_{j,t-1|j,t-1} \tag{B.53}$$

$$V_{j,t|j,t-1} = V_{j,t-1|j,t-1} + \mathbf{W}_j \tag{B.54}$$

$$K_{j,t} = V_{j,t|j,t-1}(V_{j,t|j,t-1} + \tfrac{1}{4}v_{j,t}^2)^{-1} \tag{B.55}$$

$$h_{j,t|j,t} = h_{j,t|j,t-1} + K_{j,t}(y_{j,t}^{***} - h_{j,t|j,t-1}) \tag{B.56}$$

$$V_{j,t|j,t} = V_{j,t|j,t-1} - K_{j,t}V_{j,t|j,t-1} \tag{B.57}$$

where the notation alludes to the way it was defined when drawing β_t. The backward recursions are given by:

$$h_{j,t|j,t+1} = h_{j,t|j,t} + V_{j,t|j,t}V_{j,t+1|j,t}^{-1}(h_{j,t+1} - h_{j,t|j,t}) \tag{B.58}$$

$$V_{j,t|j,t+1} = V_{j,t|j,t} - V_{j,t|j,t}V_{j,t+1|j,t}^{-1}V_{j,t|j,t} \tag{B.59}$$

Here $h_{j,t+1}$ is drawn randomly from a Normal distribution $N(h_{j,t|j,t}, V_{j,t|j,t})$ where $h_{j,t|j,t}$ and $V_{j,t|j,t}$ are taken from the calculated values during the Kalman filter step. Similarly, $V_{j,t+1|j,t} = V_{j,t|j,t} + \mathbf{W}_j$. The result is that we now have a smoothed estimates: $\beta_{t|t+1}$ and $V_{t|t+1}$. Now we finally use these means and variances to get the values of $h_{j,t}$ by randomly drawing from a Normal distribution: $N(h_{j,t|j,t+1}, V_{j,t|j,t+1})$.

B.5. Sampling hyperparameters

The covariance matrices required for the model must be recalculated every iteration. The first is the covariance of the noise term for β_t:

$$\mathbf{R}_t = A^{-1}\Sigma_t\Sigma_t'(A^{-1})'. \tag{B.60}$$

Note that the matrices are constructed from the values of α_t and h_t. The remaining hyperparameters of the model are the covariance matrices: $\mathbf{Q}$, $\mathbf{W}$ and the different diagonal blocks of $\mathbf{S}$.

In Bayesian analysis, an Inverse-Wishart distribution is often used as a prior for the covariance matrix (Gelman et al., 2013; Zhang, 2021). The Inverse-Wishart (IW) prior is also popular as it is a conjugate to normal data (that is, the posterior distribution is also normal). That is, the IW distribution gives the distribution of possible covariance matrices given m samples of data (termed as m degrees of freedom).

Conditional on and y^T, we sample the hyperparameters from the normal-inverse-Wishart distribution, with known innovations. The prior distribution of an IW distribution is given as: $IW(c_0, d_0)$, the scale and degrees of freedom of the variance covariance matrix of Q, S_i and W_j. Refer to Eqs. (B.11) to (B.14) for the prior assumptions for the hyperparameters. Given that sampling the inverse Wishart distribution is well-known via the Bartlett decomposition (Jones, 1985) implemented in modern packages (for example, scipy.stats.invwishart), we shall only present the parameters of the IW distribution required to draw the hyperparameters. The matrix $\mathbf{Q}$ associated with the random walk process for β_t can be calculated by noting that $u_t = \beta_t - \beta_{t-1}$ to randomly sample a single matrix from the IW distribution:

$$\mathbf{Q} \sim IW(\mathbf{C}_\beta + \mathbf{Q}_0, T-1) \tag{B.61}$$

$$\mathbf{C}_\beta = \sum_{t=2}^{T}(\beta_t - \beta_{t-1})(\beta_t - \beta_{t-1})', \tag{B.62}$$

where $IW(\mathbf{C}, m)$ is the IW distribution for covariance $\mathbf{C}$ and m degrees of freedom. Similarly, the matrices $\mathbf{S}_i$ associated with the random walk process α can be sampled via:

$$\mathbf{S}_i \sim IW(\mathbf{C}_\alpha, T-1) \tag{B.63}$$

$$\mathbf{C}_\alpha = \sum_{t=2}^{T}(\alpha_t - \alpha_{t-1})(\alpha_t - \alpha_{t-1})'. \tag{B.64}$$

We note that for S_1, the associated draw is from the Gamma distribution (the IW distribution for a scalar). Finally, the matrix $\mathbf{W}$ associated with the random walk process h can be sampled via:

$$\mathbf{W} \sim IW(\mathbf{C}_h, T-1) \tag{B.65}$$

$$\mathbf{C}_h = \sum_{t=2}^{T}(h_t - h_{t-1})(h_t - h_{t-1})'. \tag{B.66}$$

B.6. The MCMC algorithm

The previous sections highlighted how to draw different parameters of the TVP-VAR-SV model. The MCMC sampler repeats these draws until the parameters have converged as discussed later in Appendix C.0.1. The algorithm is summarised as:

1. Initialise A^T, Σ^T and the hyperparameters R^T, Q^T, S_i^T and W^T.
2. Sample posterior value of β^T by drawing from $N(\beta_{T|T+1}, V_{T|T+1})$.
3. Sample posterior value of A^T by drawing from $N(\alpha_{i,T|i,T+1}, V_{i,T|i,T+1})$.
4. Sample posterior values of Σ^T by drawing from $N(h_{j,T|j,T+1}, V_{j,T|j,T+1})$.
5. Sample Q^T, S_i^T and W^T by sampling from their respective Inverse Wishart distributions.
6. Repeat from Step 2.

Appendix C. MCMC simulation results

We performed the MCMC sampling on the RV data using a custom Python implementation that is available on GitHub. The algorithm was run on the ARDC Nectar cluster on a 32-core node with 64 GB RAM. The run-time was approximately 15 h. The results are shown in the main text. However, we present the raw posterior means for $\hat{\beta}_t$ and $\hat{\alpha}_t$ in Figs. C.11 and C.12.

C.0.1. Convergence tests

To ensure convergence of the posterior distributions, we run 20,000 MCMC sampling iterations of our model, from which we exclude the first 5000 iterations as burn-in and utilise the remaining 15,000 iterations to estimate the posterior values. To test if our estimated posterior distributions of the parameters have converged, we run an intuitive Cauchy convergence test to check the sum squared differences of the posterior means for every 100 iterations. If the differences in subsequent iterations become increasingly insignificant, our posterior estimates have attained convergence within an acceptable range. Fig. C.13 plots the convergence plots for the α, β and h parameters. We see that after 10000 sampling iterations, the sum squared differences drop below 0.01, while the typical sum squared values of the posterior means for the associated parameters are in the order of 10. That is, the posterior estimates fall well below 1% error.

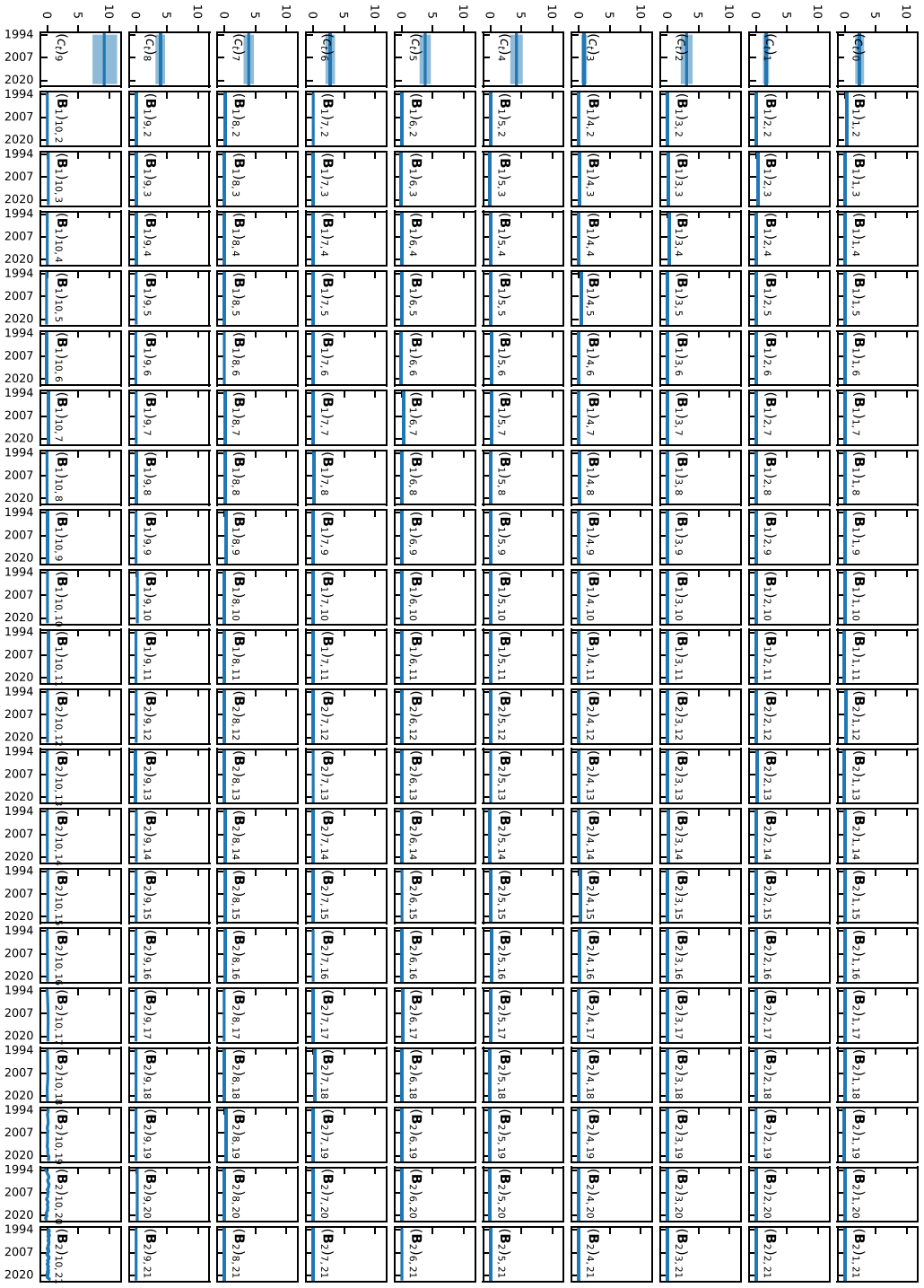

Fig. C.11. Posterior means of the time-varying constant and lagged terms of $\hat{\beta}_t$ in the VAR model.
The x-axes show the dates from Nov 93 to Feb 2022. The y-axes show the coefficient values listed inside the plots. The indices represent the asset classes in the order: Corn, Gold, Silver, SPX, Crude oil, Heating oil, Copper, Lumber, Wheat, Natural Gas. The error bars represent the variation within 5th and 95th percentile values of the terms.

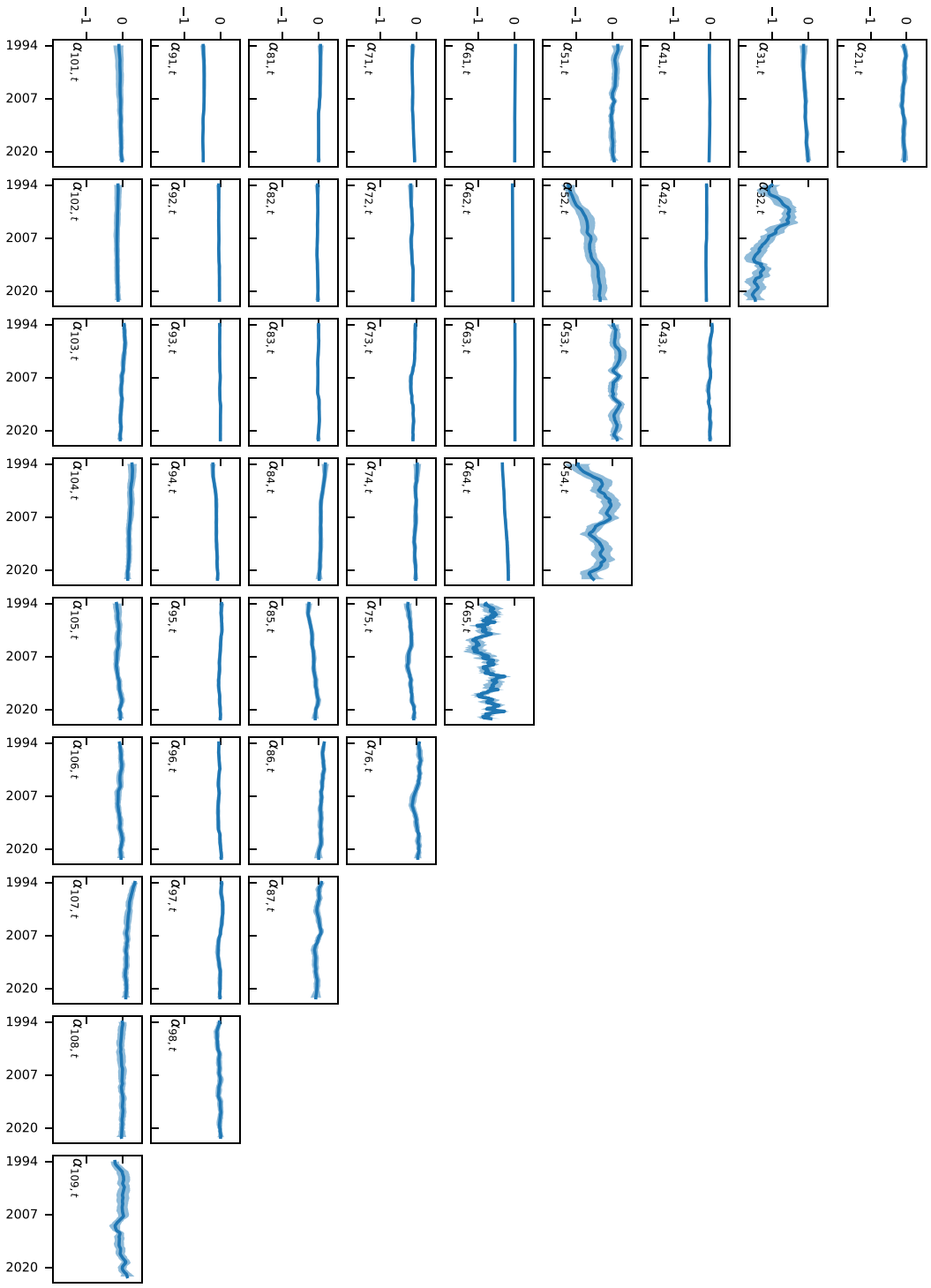

Fig. C.12. Posterior means of the time-varying contemporaneous terms $\hat{a}_t$ in the VAR model.
The x-axes show the dates from Nov 93 to Feb 2022. The y-axes show the coefficient values listed inside the plots. The indices represent the asset classes in the order: Corn, Gold, Silver, SPX, Crude oil, Heating oil, Copper, Lumber, Wheat, Natural Gas. The error bars represent the variation within 5th and 95th percentile values of the terms.

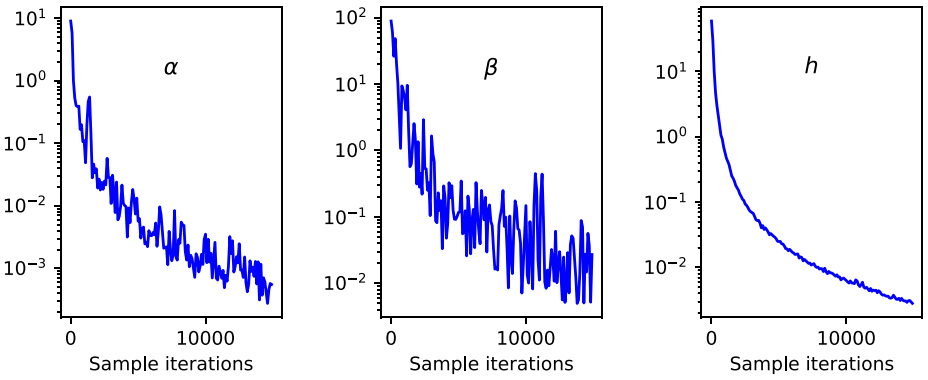

Fig. C.13. Convergence test for the posterior means of the time-varying parameters.
The x-axes indicate the number of completed MCMC iterations. The y-axes show the sum of squared differences in the posterior means of the parameters for every 100 iterations. The *y* axes are scaled logarithmically to better visualise the decay when the sum differences of the square of posterior means between successive 100 iterations become more and more indistinguishable.

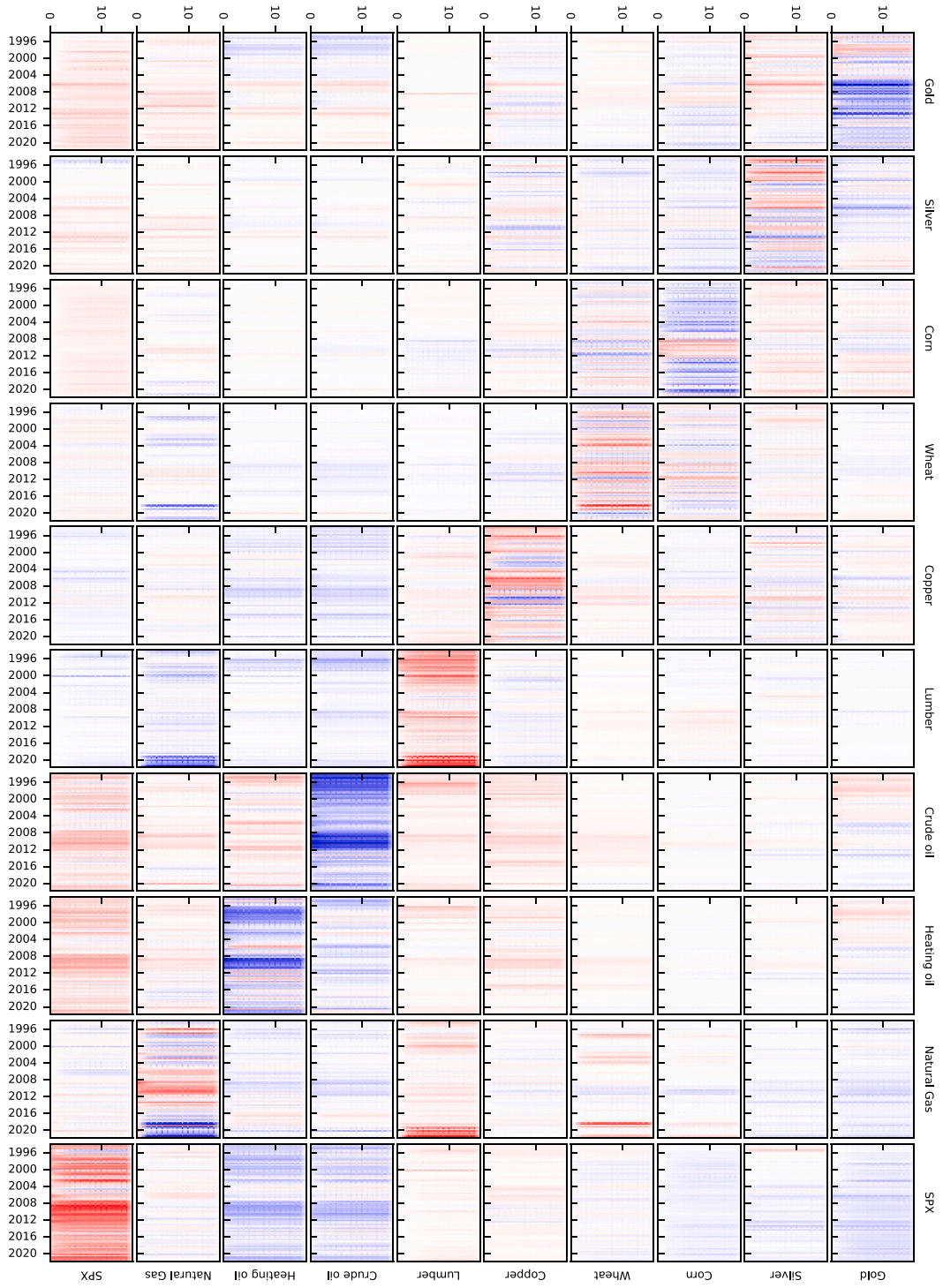

Fig. C.14. Net pair-wise volatility spillover index across horizons H=1 to 16.
The Figure illustrates the net pairwise spillover index for variance decomposition periods H= 1 to 16. Details of the shaded crisis periods are mentioned in Table 2. The X axes show the extent of volatility spillover. The Y axes show the dates from Nov 93 to Oct 2021. The red lines represent positive net spillover (net transmitter) from column i to row j. The blue lines represent negative net spillover (net receiver) from column i to row j. The off diagonal elements plot the net pairwise spillover index defined in Eq. (13). The diagonal elements plot net volatility spillover to the remaining asset classes defined in Eq. (14). The off-diagonals mirror one another up to a sign of −1. (For interpretation of the references to colour in this figure legend, the reader is referred to the web version of this article.)

C.1. Horizon saturation

We compute the pair-wise time-varying net spillover index, for variance decomposition periods H = 1 to 16. Fig. C.14 plots the net volatility spillover indices for horizon periods H = 1to16. We find that beyond variance decomposition period $H = 8$, the spillover effects have already saturated to their maximum values.

Data availability

Data and associated code will be provided upon request.

References

Abdullah, M., Chowdhury, M.A.F., Sulong, Z., 2023. Asymmetric efficiency and connectedness among green stocks, halal tourism stocks, cryptocurrencies, and commodities: Portfolio hedging implications. Resour. Policy 81, 103419. http://dx.doi.org/10.1016/j.resourpol.2023.103419.

Adekoya, O.B., Akinseye, A.B., Antonakakis, N., Chatziantoniou, I., Gabauer, D., Oliyide, J., 2022. Crude oil and islamic sectoral stocks: Asymmetric TVP-VAR connectedness and investment strategies. Resour. Policy 78, 102877. http://dx.doi.org/10.1016/j.resourpol.2022.102877.

Adelman, M.A., 1984. International oil agreements. Energy J. 5 (3), 1–9, URL: http://www.jstor.org/stable/41321691.

Ahmed, A.D., Huo, R., 2021. Volatility transmissions across international oil market, commodity futures and stock markets: Empirical evidence from China. Energy Econ. 93, 104741. http://dx.doi.org/10.1016/j.eneco.2020.104741.

Akca, K., Ozturk, S.S., 2015. The effect of 2008 crisis on the volatility spillovers among six major markets. Int. Rev. Financ. 16 (1), 169–178. http://dx.doi.org/10.1111/irfi.12071.

Akhtaruzzaman, M., Boubaker, S., Lucey, B.M., Sensoy, A., 2021. Is gold a hedge or a safe-haven asset in the COVID–19 crisis? Econ. Model. 102, 105588. http://dx.doi.org/10.1016/j.econmod.2021.105588.

Andersen, T.G., Bollerslev, T., 1998. Answering the skeptics: Yes, standard volatility models do provide accurate forecasts. Internat. Econom. Rev. 39 (4), 885. http://dx.doi.org/10.2307/2527343.

Andersen, T.G., Bollerslev, T., Diebold, F.X., Labys, P., 2003. Modeling and forecasting realized volatility. Econometrica 71 (2), 579–625. http://dx.doi.org/10.1111/1468-0262.00418.

Arellano, C., Conesa, J.C., Kehoe, T.J., 2012. Chronic sovereign debt crises in the Eurozone, 2010–2012. Fed. Reserv. Bank Minneap. Econ. Policy Pap. 12 (04).

Asadi, M., Roubaud, D., Tiwari, A.K., 2022. Volatility spillovers amid crude oil, natural gas, coal, stock, and currency markets in the US and China based on time and frequency domain connectedness. Energy Econ. 109, 105961. http://dx.doi.org/10.1016/j.eneco.2022.105961.

Baele, L., 2005. Volatility spillover effects in European equity markets. J. Financ. Quant. Anal. 40 (2), 373–401. http://dx.doi.org/10.1017/s0022109000002350.

Bai, L., Wei, Y., Zhang, J., Wang, Y., Lucey, B.M., 2023. Diversification effects of China's carbon neutral bond on renewable energy stock markets: A minimum connectedness portfolio approach. Energy Econ. 123, 106727. http://dx.doi.org/10.1016/j.eneco.2023.106727.

Balcilar, M., Hammoudeh, S., Toparli, E.A., 2018. On the risk spillover across the oil market, stock market, and the oil related CDS sectors: A volatility impulse response approach. Energy Econ. 74, 813–827. http://dx.doi.org/10.1016/j.eneco.2018.07.027.

Balcilar, M., Ozdemir, Z.A., Ozdemir, H., 2019. Dynamic return and volatility spillovers among S&P 500, crude oil, and gold. Int. J. Financ. Econ. 26 (1), 153–170. http://dx.doi.org/10.1002/ijfe.1782.

Basak, S., Pavlova, A., 2016. A model of financialization of commodities. J. Financ. 71 (4), 1511–1556. http://dx.doi.org/10.1111/jofi.12408.

Batten, J.A., Kinateder, H., Szilagyi, P.G., Wagner, N.F., 2019. Time-varying energy and stock market integration in Asia. Energy Econ. 80, 777–792. http://dx.doi.org/10.1016/j.eneco.2019.01.008.

Baur, D.G., Kuck, K., 2020. The timing of the flight to gold: An intra-day analysis of gold and the S&P500. Financ. Res. Lett. 33, 101187. http://dx.doi.org/10.1016/j.frl.2019.05.005.

Baur, D.G., McDermott, T.K., 2010. Is gold a safe haven? International evidence. J. Bank. Financ. 34 (8), 1886–1898. http://dx.doi.org/10.1016/j.jbankfin.2009.12.008.

Baur, D.G., Trench, A., 2022. Not all gold shines in crisis times — Gold firms, gold bullion and the COVID-19 shock. J. Commod. Mark. 28, 100260. http://dx.doi.org/10.1016/j.jcomm.2022.100260.

Bekaert, G., Harvey, C., 2003. Market Integration and Contagion. National Bureau of Economic Research, http://dx.doi.org/10.3386/w9510.

Benlagha, N., Karim, S., Naeem, M.A., Lucey, B.M., Vigne, S.A., 2022. Risk connectedness between energy and stock markets: Evidence from oil importing and exporting countries. Energy Econ. 115, 106348. http://dx.doi.org/10.1016/j.eneco.2022.106348.

Bhar, R., Nikolova, B., 2009. Return, volatility spillovers and dynamic correlation in the BRIC equity markets: An analysis using a bivariate EGARCH framework. Glob. Financ. J. 19 (3), 203–218. http://dx.doi.org/10.1016/j.gfj.2008.09.005.

Bianchi, R.J., Fan, J.H., Todorova, N., 2020. Financialization and de-financialization of commodity futures: A quantile regression approach. Int. Rev. Financ. Anal. 68, 101451. http://dx.doi.org/10.1016/j.irfa.2019.101451.

Black, F., 1976. Studies of stock price volatility changes. In: Proceedings of the 1976 Meeting of the Business and Economic Statistics Section. American Statistical Association, pp. 177–181. http://dx.doi.org/10.1002/fut.22086.

Bouri, E., Lei, X., Jalkh, N., Xu, Y., Zhang, H., 2021a. Spillovers in higher moments and jumps across US stock and strategic commodity markets. Resour. Policy 72, 102060. http://dx.doi.org/10.1016/j.resourpol.2021.102060.

Bouri, E., Lucey, B., Saeed, T., Vo, X.V., 2021b. The realized volatility of commodity futures: Interconnectedness and determinants. Int. Rev. Econ. Financ. 73, 139–151. http://dx.doi.org/10.1016/j.iref.2021.01.006.

Broadstock, D., Chatziantoniou, I., Gabauer, D., 2020. Minimum connectedness portfolios and the market for green bonds: Advocating socially responsible investment (SRI) activity. SSRN Electron. J. http://dx.doi.org/10.2139/ssrn.3793771.

Buccioli, A., Kokholm, T., 2021. Shock waves and golden shores: the asymmetric interaction between gold prices and the stock market. Eur. J. Financ. 28 (7), 743–760. http://dx.doi.org/10.1080/1351847x.2021.1897026.

Burdekin, R.C., Tao, R., 2021. The golden hedge: From global financial crisis to global pandemic. Econ. Model. 95, 170–180. http://dx.doi.org/10.1016/j.econmod.2020.12.009.

Burmeister, E., Wall, K.D., Hamilton, J.D., 1986. Estimation of unobserved expected monthly inflation using Kalman filtering. J. Bus. Econom. Statist. 4 (2), 147–160. http://dx.doi.org/10.1080/07350015.1986.10509510.

Cabrera, B.L., Schulz, F., 2016. Volatility linkages between energy and agricultural commodity prices. Energy Econ. 54, 190–203. http://dx.doi.org/10.1016/j.eneco.2015.11.018.

Caporale, G.M., Pittis, N., Spagnolo, N., 2006. Volatility transmission and financial crises. J. Econ. Financ. 30 (3), 376–390. http://dx.doi.org/10.1007/bf02752742.

Caporin, M., Fontini, F., 2017. The long-run oil–natural gas price relationship and the shale gas revolution. Energy Econ. 64, 511–519. http://dx.doi.org/10.1016/j.eneco.2016.07.024.

Carter, C.K., Kohn, R., 1994. On Gibbs sampling for state space models. Biometrika 81 (3), 541–553. http://dx.doi.org/10.1093/biomet/81.3.541.

Chan, J.C.C., Eisenstat, E., 2018. Bayesian model comparison for time-varying parameter VARs with stochastic volatility. J. Appl. Econometrics 33 (4), 509–532. http://dx.doi.org/10.1002/jae.2617.

Chang, C.L., McAleer, M., Tansuchat, R., 2010. Analyzing and forecasting volatility spillovers, asymmetries and hedging in major oil markets. Energy Econ. 32 (6), 1445–1455. http://dx.doi.org/10.1016/j.eneco.2010.04.014.

Chen, J., Liang, Z., Ding, Q., Ren, X., Wu, A., 2023. Dynamic connectedness across energy and metal futures markets during the COVID-19 pandemic: New evidence from a time-varying spillover index. Resour. Policy 86, 104249. http://dx.doi.org/10.1016/j.resourpol.2023.104249.

Clarke, R., De Silva, H., Thorley, S., 2011. Minimum-variance portfolio composition. J. Portf. Manag. 37 (2), 31.

Cogley, T., Sargent, T.J., 2005. Drifts and volatilities: monetary policies and outcomes in the post WWII US. Rev. Econ. Dyn. 8 (2), 262–302. http://dx.doi.org/10.1016/j.red.2004.10.009.

Corbet, S., Hou, Y.G., Hu, Y., Oxley, L., 2021. Volatility spillovers during market supply shocks: The case of negative oil prices. Resour. Policy 74, 102357. http://dx.doi.org/10.1016/j.resourpol.2021.102357.

Creti, A., Nguyen, D.K., 2015. Energy markets' financialization, risk spillovers, and pricing models. Energy Policy 82, 260–263. http://dx.doi.org/10.1016/j.enpol.2015.02.007.

DeMiguel, V., Garlappi, L., Uppal, R., 2007. Optimal versus naive diversification: How inefficient is the 1/NPortfolio strategy? Rev. Financ. Stud. 22 (5), 1915–1953. http://dx.doi.org/10.1093/rfs/hhm075.

Diebold, F.X., Yilmaz, K., 2008. Measuring financial asset return and volatility spillovers, with application to global equity markets. Econ. J. 119 (534), 158–171. http://dx.doi.org/10.1111/j.1468-0297.2008.02208.x.

Diebold, F.X., Yilmaz, K., 2012. Better to give than to receive: Predictive directional measurement of volatility spillovers. Int. J. Forecast. 28 (1), 57–66. http://dx.doi.org/10.1016/j.ijforecast.2011.02.006.

Diebold, F.X., Yılmaz, K., 2014. On the network topology of variance decompositions: Measuring the connectedness of financial firms. J. Econometrics 182 (1), 119–134. http://dx.doi.org/10.1016/j.jeconom.2014.04.012.

Ederington, L.H., 1979. The hedging performance of the new futures markets. J. Financ. 34 (1), 157–170. http://dx.doi.org/10.1111/j.1540-6261.1979.tb02077.x.

Ehrmann, M., Fratzscher, M., 2017. Euro area government bonds – Fragmentation and contagion during the sovereign debt crisis. J. Int. Money Financ. 70, 26–44. http://dx.doi.org/10.1016/j.jimonfin.2016.08.005.

Elsayed, A.H., Hoque, M.E., Billah, M., Alam, M.K., 2024. Connectedness across meme assets and sectoral markets: Determinants and portfolio management. Int. Rev. Financ. Anal. 93, 103177. http://dx.doi.org/10.1016/j.irfa.2024.103177.

Erb, C.B., Harvey, C.R., 2006. The strategic and tactical value of commodity futures. Financ. Anal. J. 62 (2), 69–97. http://dx.doi.org/10.2469/faj.v62.n2.4084.

Erdős, P., 2012. Have oil and gas prices got separated? Energy Policy 49, 707–718. http://dx.doi.org/10.1016/j.enpol.2012.07.022.

Fantazzini, D., 2016. The oil price crash in 2014/15: Was there a (negative) financial bubble? Energy Policy 96, 383–396. http://dx.doi.org/10.1016/j.enpol.2016.06.020.

Farid, S., Kayani, G.M., Naeem, M.A., Shahzad, S.J.H., 2021. Intraday volatility transmission among precious metals, energy and stocks during the COVID-19 pandemic. Resour. Policy 72, 102101. http://dx.doi.org/10.1016/j.resourpol.2021.102101.

Farid, S., Naeem, M.A., Paltrinieri, A., Nepal, R., 2022. Impact of COVID-19 on the quantile connectedness between energy, metals and agriculture commodities. Energy Econ. 109, 105962. http://dx.doi.org/10.1016/j.eneco.2022.105962.

Filis, G., Degiannakis, S., Floros, C., 2011. Dynamic correlation between stock market and oil prices: The case of oil-importing and oil-exporting countries. Int. Rev. Financ. Anal. 20 (3), 152–164. http://dx.doi.org/10.1016/j.irfa.2011.02.014.

Fuller, W.A., 1995. Introduction to Statistical Time Series, second ed. Wiley.

Gelman, A., Carlin, J.B., Stern, H.S., Dunson, D.B., Vehtari, A., Rubin, D.B., 2013. Bayesian Data Analysis, third ed. In: Chapman & Hall/CRC Texts in Statistical Science, Chapman & Hall/CRC, Philadelphia, PA.

Gong, X., Jin, Y., Sun, C., 2022a. Time-varying pure contagion effect between energy and nonenergy commodity markets. J. Futur. Mark. 42 (10), 1960–1986. http://dx.doi.org/10.1002/fut.22366.

Gong, X., Liu, Y., Wang, X., 2021. Dynamic volatility spillovers across oil and natural gas futures markets based on a time-varying spillover method. Int. Rev. Financ. Anal. 76, 101790. http://dx.doi.org/10.1016/j.irfa.2021.101790.

Gong, X., Xu, J., 2022. Geopolitical risk and dynamic connectedness between commodity markets. Energy Econ. 110, 106028. http://dx.doi.org/10.1016/j.eneco.2022.106028.

Gong, X., Xu, J., Liu, T., Zhou, Z., 2022b. Dynamic volatility connectedness between industrial metal markets. North Am. J. Econ. Financ. 63, 101814. http://dx.doi.org/10.1016/j.najef.2022.101814.

Gorton, G., Rouwenhorst, K.G., 2006. Facts and fantasies about commodity futures. Financ. Anal. J. 62 (2), 47–68. http://dx.doi.org/10.2469/faj.v62.n2.4083.

Gozgor, G., Lau, C.K.M., Bilgin, M.H., 2016. Commodity markets volatility transmission: Roles of risk perceptions and uncertainty in financial markets. J. Int. Financ. Mark. Inst. Money 44, 35–45. http://dx.doi.org/10.1016/j.intfin.2016.04.008.

Greene, W.H., 2022. Econometric analysis. ISBN: 9780130661890.

Gülen, S.G., 1997. Regionalization in the world crude oil market. Energy J. 18 (2), 109–126, URL: http://www.jstor.org/stable/41322733.

Hamilton, J., 2011. Historical Oil Shocks. Technical Report, National Bureau of Economic Research, http://dx.doi.org/10.3386/w16790.

Heiden, M.D., 2015. Pitfalls of the Cholesky decomposition for forecasting multivariate volatility. SSRN Electron. J. http://dx.doi.org/10.2139/ssrn.2686482.

Hung, N.T., 2021. Oil prices and agricultural commodity markets: Evidence from pre and during COVID-19 outbreak. Resour. Policy 73, 102236. http://dx.doi.org/10.1016/j.resourpol.2021.102236.

Jebabli, I., Kouaissah, N., Arouri, M., 2022. Volatility spillovers between stock and energy markets during crises: A comparative assessment between the 2008 global financial crisis and the Covid-19 pandemic crisis. Financ. Res. Lett. 46, 102363. http://dx.doi.org/10.1016/j.frl.2021.102363.

Jones, M.C., 1985. Generating inverse wishart matrices. Comm. Statist. Simulation Comput. 14 (2), 511–514. http://dx.doi.org/10.1080/03610918508812454.

Joo, K., Suh, J.H., Lee, D., Ahn, K., 2020. Impact of the global financial crisis on the crude oil market. Energy Strat. Rev. 30, 100516. http://dx.doi.org/10.1016/j.esr.2020.100516.

Kalman, R.E., 1960. A new approach to linear filtering and prediction problems. J. Basic Eng. 82 (1), 35–45. http://dx.doi.org/10.1115/1.3662552.

Kamal, M.M., Roca, E., Li, B., Lin, C., Reza, R., 2021. Price contagion and risk spillover in the global commodities market: COVID-19 pandemic vs. Global financial crisis. SSRN Electron. J. http://dx.doi.org/10.2139/ssrn.4039083.

Kaminsky, G.L., Schmukler, S.L., 1999. What triggers market jitters? J. Int. Money Financ. 18 (4), 537–560. http://dx.doi.org/10.1016/s0261-5606(99)00015-7.

Kang, S.H., McIver, R., Yoon, S.M., 2017. Dynamic spillover effects among crude oil, precious metal, and agricultural commodity futures markets. Energy Econ. 62, 19–32. http://dx.doi.org/10.1016/j.eneco.2016.12.011.

Kang, W., Tang, K., Wang, N., 2023. Financialization of commodity markets ten years later. J. Commod. Mark. 30, 100313. http://dx.doi.org/10.1016/j.jcomm.2023.100313.

Kang, S.H., Yoon, S., 2019. Dynamic correlation and volatility spillovers across Chinese stock and commodity futures markets. Int. J. Financ. Econ. 25 (2), 261–273. http://dx.doi.org/10.1002/ijfe.1750.

Khalfaoui, R., Sarwar, S., Tiwari, A.K., 2019. Analysing volatility spillover between the oil market and the stock market in oil-importing and oil-exporting countries: Implications on portfolio management. Resour. Policy 62, 22–32. http://dx.doi.org/10.1016/j.resourpol.2019.03.004.

Kilian, L., 2016. The impact of the shale oil revolution on U.S. oil and gasoline prices. SSRN Electron. J. http://dx.doi.org/10.2139/ssrn.2743100.

Kim, S., Shepherd, N., Chib, S., 1998. Stochastic volatility: Likelihood inference and comparison with ARCH models. Rev. Econ. Stud. 65 (3), 361–393. http://dx.doi.org/10.1111/1467-937x.00050.

Klein, T., 2017. Dynamic correlation of precious metals and flight-to-quality in developed markets. Financ. Res. Lett. 23, 283–290. http://dx.doi.org/10.1016/j.frl.2017.05.002.

Koop, G.M., 2011. Forecasting with medium and large Bayesian VARS. J. Appl. Econometrics 28 (2), 177–203. http://dx.doi.org/10.1002/jae.1270.

Korobilis, D.m., Yilmaz, K.m., 2018. Measuring dynamic connectedness with large Bayesian VAR models. SSRN Electron. J. http://dx.doi.org/10.2139/ssrn.3099725.

Krugman, P.R., 2000. Currency crises. In: National Bureau of Economic Research Conference Report, University of Chicago Press, Chicago, IL.

Lien, D., Lee, G., Yang, L., Zhang, Y., 2018. Volatility spillovers among the U.S. and Asian stock markets: A comparison between the periods of Asian currency crisis and subprime credit crisis. North Am. J. Econ. Financ. 46, 187–201. http://dx.doi.org/10.1016/j.najef.2018.04.006.

Lin, S.X., Tamvakis, M.N., 2001. Spillover effects in energy futures markets. Energy Econ. 23 (1), 43–56. http://dx.doi.org/10.1016/s0140-9883(00)00051-7.

Liow, K.H., 2015. Volatility spillover dynamics and relationship across G7 financial markets. North Am. J. Econ. Financ. 33, 328–365. http://dx.doi.org/10.1016/j.najef.2015.06.003.

Liu, T., Gong, X., 2020. Analyzing time-varying volatility spillovers between the crude oil markets using a new method. Energy Econ. 87, 104711. http://dx.doi.org/10.1016/j.eneco.2020.104711.

Liu, T., Gong, X., Lin, B., 2021. Analyzing the frequency dynamics of volatility spillovers across precious and industrial metal markets. J. Futur. Mark. 41 (9), 1375–1396. http://dx.doi.org/10.1002/fut.22217.

Liu, C., Zhang, X., Zhou, Z., 2023. Are commodity futures a hedge against inflation? A Markov-switching approach. Int. Rev. Financ. Anal. 86, 102492. http://dx.doi.org/10.1016/j.irfa.2023.102492.

Lovcha, Y., Perez-Laborda, A., 2020. Dynamic frequency connectedness between oil and natural gas volatilities. Econ. Model. 84, 181–189. http://dx.doi.org/10.1016/j.econmod.2019.04.008.

Lubik, T.A., Matthes, C., 2016. Time-varying parameter vector autoregressions: Specification, estimation, and an application. Econ. Q. 101 (04), 323–352. http://dx.doi.org/10.21144/eq1010403.

Lucey, B.M., Li, S., 2014. What precious metals act as safe havens, and when? Some US evidence. Appl. Econ. Lett. 22 (1), 35–45. http://dx.doi.org/10.1080/13504851.2014.920471.

Lütkepohl, H., 2005. New introduction to multiple time series analysis.

Maghyereh, A.I., Awartani, B., Bouri, E., 2016. The directional volatility connectedness between crude oil and equity markets: New evidence from implied volatility indexes. Energy Econ. 57, 78–93. http://dx.doi.org/10.1016/j.eneco.2016.04.010.

Maillard, S., Roncalli, T., Teïletche, J., 2010. The properties of equally weighted risk contribution portfolios. J. Portf. Manag. 36 (4), 60.

Main, S., Irwin, S.H., Sanders, D.R., Smith, A., 2018. Financialization and the returns to commodity investments. J. Commod. Mark. 10, 22–28. http://dx.doi.org/10.1016/j.jcomm.2018.05.004.

Malik, F., Hammoudeh, S., 2007. Shock and volatility transmission in the oil, US and gulf equity markets. Int. Rev. Econ. Financ. 16 (3), 357–368. http://dx.doi.org/10.1016/j.iref.2005.05.005.

Mandacı, P.E., Cagli, E.Ç., Taşkın, D., 2020. Dynamic connectedness and portfolio strategies: Energy and metal markets. Resour. Policy 68, 101778. http://dx.doi.org/10.1016/j.resourpol.2020.101778.

Markowitz, H.M., 1959. Portfolio Selection: Efficient Diversification of Investments. Yale University Press, URL: http://www.jstor.org/stable/j.ctt1bh4c8h.

McMillan, D.G., Speight, A.E., 2010. Return and volatility spillovers in three euro exchange rates. J. Econ. Bus. 62 (2), 79–93. http://dx.doi.org/10.1016/j.jeconbus.2009.08.003.

Mensi, W., Al Rababa'a, A.R., Vo, X.V., Kang, S.H., 2021a. Asymmetric spillover and network connectedness between crude oil, gold, and Chinese sector stock markets. Energy Econ. 98, 105262. http://dx.doi.org/10.1016/j.eneco.2021.105262.

Mensi, W., Al-Yahyaee, K.H., Hoon Kang, S., 2017. Time-varying volatility spillovers between stock and precious metal markets with portfolio implications. Resour. Policy 53, 88–102. http://dx.doi.org/10.1016/j.resourpol.2017.06.001.

Mensi, W., Aslan, A., Vo, X.V., Kang, S.H., 2023. Time-frequency spillovers and connectedness between precious metals, oil futures and financial markets: Hedge and safe haven implications. Int. Rev. Econ. Financ. 83, 219–232. http://dx.doi.org/10.1016/j.iref.2022.08.015.

Mensi, W., Boubaker, F.Z., Al-Yahyaee, K.H., Kang, S.H., 2018. Dynamic volatility spillovers and connectedness between global, regional, and GIPSI stock markets. Financ. Res. Lett. 25, 230–238. http://dx.doi.org/10.1016/j.frl.2017.10.032.

Mensi, W., Hammoudeh, S., Vinh Vo, X., Hoon Kang, S., 2021b. Volatility spillovers between oil and equity markets and portfolio risk implications in the US and vulnerable EU countries. J. Int. Financ. Mark. Inst. Money 75, 101457. http://dx.doi.org/10.1016/j.intfin.2021.101457.

Mensi, W., Rehman, M.U., Vo, X.V., 2020. Spillovers and co-movements between precious metals and energy markets: Implications on portfolio management. Resour. Policy 69, 101836. http://dx.doi.org/10.1016/j.resourpol.2020.101836.

Mensi, W., Rehman, M.U., Vo, X.V., 2021c. Dynamic frequency relationships and volatility spillovers in natural gas, crude oil, gas oil, gasoline, and heating oil markets: Implications for portfolio management. Resour. Policy 73, 102172. http://dx.doi.org/10.1016/j.resourpol.2021.102172.

Mensi, W., Shafiullah, M., Vo, X.V., Kang, S.H., 2021d. Volatility spillovers between strategic commodity futures and stock markets and portfolio implications: Evidence from developed and emerging economies. Resour. Policy 71, 102002. http://dx.doi.org/10.1016/j.resourpol.2021.102002.

Miffre, J., Rallis, G., 2007. Momentum strategies in commodity futures markets. J. Bank. Financ. 31 (6), 1863–1886. http://dx.doi.org/10.1016/j.jbankfin.2006.12.005.

Miyazaki, T., Hamori, S., 2013. Testing for causality between the gold return and stock market performance: evidence for 'gold investment in case of emergency'. Appl. Financ. Econ. 23 (1), 27–40. http://dx.doi.org/10.1080/09603107.2012.699184.

Nakajima, J., 2011. Time-varying parameter VAR model with stochastic volatility: An overview of methodology and empirical applications. Monet. Econ. Stud. 29, 107–142, URL: https://EconPapers.repec.org/RePEc:ime:imemes:v:29:y:2011:p:107-142.

Negro, M.D., Primiceri, G.E., 2015. Time varying structural vector autoregressions and monetary policy: A corrigendum. Rev. Econ. Stud. 82 (4), 1342–1345. http://dx.doi.org/10.1093/restud/rdv024.

Nguyen, D.K., Sensoy, A., Sousa, R.M., Uddin, G.S., 2020. U.S. equity and commodity futures markets: Hedging or financialization? Energy Econ. 86, 104660. http://dx.doi.org/10.1016/j.eneco.2019.104660.

Niu, H., Hu, W., 2024. Static and dynamic interdependencies among natural gas, stocks of global major economies and uncertainty. Resour. Policy 94, 105101. http://dx.doi.org/10.1016/j.resourpol.2024.105101.

Okhrin, Y., Uddin, G.S., Yahya, M., 2023. Nonlinear and asymmetric interconnectedness of crude oil with financial and commodity markets. Energy Econ. 125, 106853. http://dx.doi.org/10.1016/j.eneco.2023.106853.

Pindyck, R.S., 2004. Volatility in natural gas and oil markets. J. Energy Dev. 30, 1.

Primiceri, G.E., 2005. Time varying structural vector autoregressions and monetary policy. Rev. Econ. Stud. 72 (3), 821–852. http://dx.doi.org/10.1111/j.1467-937x.2005.00353.x.

Qiao, T., Han, L., 2022. COVID-19 and tail risk contagion across commodity futures markets. J. Futur. Mark. 43 (2), 242–272. http://dx.doi.org/10.1002/fut.22388.

Ramberg, D.J., Parsons, J.E., 2012. The weak tie between natural gas and oil prices. Energy J. 33 (2), http://dx.doi.org/10.5547/01956574.33.2.2.

Rehman, M.U., Vo, X.V., 2021. Energy commodities, precious metals and industrial metal markets: A nexus across different investment horizons and market conditions. Resour. Policy 70, 101843. http://dx.doi.org/10.1016/j.resourpol.2020.101843.

Rizvi, S.K.A., Naqvi, B., Boubaker, S., Mirza, N., 2022. The power play of natural gas and crude oil in the move towards the financialization of the energy market. Energy Econ. 112, 106131. http://dx.doi.org/10.1016/j.eneco.2022.106131.

Rovenpor, 2003. Explaining the E-commerce shakeout: Why did so many internet-based businesses fail? E- Serv. J. 3 (1), 53. http://dx.doi.org/10.2979/esj.2003.3.1.53.

Sarwar, S., Tiwari, A.K., Tingqiu, C., 2020. Analyzing volatility spillovers between oil market and Asian stock markets. Resour. Policy 66, 101608. http://dx.doi.org/10.1016/j.resourpol.2020.101608.

Sehgal, S., Rajput, N., Deisting, F., 2013. Price Discovery and Volatility Spillover: Evidence from Indian Commodity Markets. Int. J. Bus. Financ. Res. 7 (3), 57–75, URL: https://papers.ssrn.com/sol3/papers.cfm?abstract_id=2149790.

Serra, T., 2011. Volatility spillovers between food and energy markets: A semiparametric approach. Energy Econ. 33 (6), 1155–1164. http://dx.doi.org/10.1016/j.eneco.2011.04.003.

Sims, C.A., Zha, T., 2006. Were there regime switches in U.S. monetary policy? Am. Econ. Rev. 96 (1), 54–81. http://dx.doi.org/10.1257/000282806776157678.

Smales, L., 2021. Geopolitical risk and volatility spillovers in oil and stock markets. Q. Rev. Econ. Financ. 80, 358–366. http://dx.doi.org/10.1016/j.qref.2021.03.008.

Spierdijk, L., Umar, Z., 2010. Are commodities a good hedge against inflation? A comparative approach. SSRN Electron. J. http://dx.doi.org/10.2139/ssrn.1730243.

Sun, C., Min, J., Sun, J., Gong, X., 2023. The role of China's crude oil futures in world oil futures market and China's financial market. Energy Econ. 120, 106619. http://dx.doi.org/10.1016/j.eneco.2023.106619.

Syriopoulos, T., Makram, B., Boubaker, A., 2015. Stock market volatility spillovers and portfolio hedging: BRICS and the financial crisis. Int. Rev. Financ. Anal. 39, 7–18. http://dx.doi.org/10.1016/j.irfa.2015.01.015.

Szafranek, K., Rubaszek, M., Uddin, G.S., 2024. The role of uncertainty and sentiment for intraday volatility connectedness between oil and financial markets. Energy Econ. 137, 107760. http://dx.doi.org/10.1016/j.eneco.2024.107760.

Tiwari, A.K., Abakah, E.J.A., Adewuyi, A.O., Lee, C.C., 2022. Quantile risk spillovers between energy and agricultural commodity markets: Evidence from pre and during COVID-19 outbreak. Energy Econ. 113, 106235. http://dx.doi.org/10.1016/j.eneco.2022.106235.

Umar, Z., Jareño, F., Escribano, A., 2021. Oil price shocks and the return and volatility spillover between industrial and precious metals. Energy Econ. 99, 105291. http://dx.doi.org/10.1016/j.eneco.2021.105291.

Wang, X., Wu, C., 2018. Asymmetric volatility spillovers between crude oil and international financial markets. Energy Econ. 74, 592–604. http://dx.doi.org/10.1016/j.eneco.2018.06.022.

Wang, H., Yuan, Y., Wang, T., 2021. The dynamics of cross-boundary fire—Financial contagion between the oil and stock markets. J. Futur. Mark. 41 (10), 1655–1673. http://dx.doi.org/10.1002/fut.22239.

Weiner, R.J., 1991. Is the world oil market "One great pool"? Energy J. 12 (3), 95–107, URL: http://www.jstor.org/stable/41322430.

Wen, X., Wei, Y., Huang, D., 2012. Measuring contagion between energy market and stock market during financial crisis: A copula approach. Energy Econ. 34 (5), 1435–1446. http://dx.doi.org/10.1016/j.eneco.2012.06.021.

Xiao, B., Yu, H., Fang, L., Ding, S., 2019. Estimating the connectedness of commodity futures using a network approach. J. Futur. Mark. 40 (4), 598–616. http://dx.doi.org/10.1002/fut.22086.

Xu, Y., Guan, B., Lu, W., Heravi, S., 2024. Macroeconomic shocks and volatility spillovers between stock, bond, gold and crude oil markets. Energy Econ. 136, 107750. http://dx.doi.org/10.1016/j.eneco.2024.107750.

Xu, W., Ma, F., Chen, W., Zhang, B., 2019. Asymmetric volatility spillovers between oil and stock markets: Evidence from China and the United States. Energy Econ. 80, 310–320. http://dx.doi.org/10.1016/j.eneco.2019.01.014.

Xu, Y., Taylor, N., Lu, W., 2018. Illiquidity and volatility spillover effects in equity markets during and after the global financial crisis: An MEM approach. Int. Rev. Financ. Anal. 56, 208–220. http://dx.doi.org/10.1016/j.irfa.2018.01.011.

Yang, J., Geng, J.B., Liang, Z., 2024. Time-varying effects of structural oil price shocks on financial market uncertainty. Energy Econ. 139, 107910. http://dx.doi.org/10.1016/j.eneco.2024.107910.

Yang, J., Li, Z., Miao, H., 2021. Volatility spillovers in commodity futures markets: A network approach. J. Futur. Mark. 41 (12), 1959–1987. http://dx.doi.org/10.1002/fut.22270.

Yıldırım, D.Ç., Cevik, E.I., Esen, Ö., 2020. Time-varying volatility spillovers between oil prices and precious metal prices. Resour. Policy 68, 101783. http://dx.doi.org/10.1016/j.resourpol.2020.101783.

Yip, P.S., Brooks, R., Do, H.X., Nguyen, D.K., 2020. Dynamic volatility spillover effects between oil and agricultural products. Int. Rev. Financ. Anal. 69, 101465. http://dx.doi.org/10.1016/j.irfa.2020.101465.

Zhang, Z., 2021. A note on wishart and inverse wishart priors for covariance matrix. J. Behav. Data Sci. 1 (2), http://dx.doi.org/10.35566/jbds/v1n2/p2.

Zhang, D., Broadstock, D.C., 2020. Global financial crisis and rising connectedness in international commodity markets. Int. Rev. Financ. Anal. 68, 101239. http://dx.doi.org/10.1016/j.irfa.2018.08.003.

Zhang, Y.J., Chevallier, J., Guesmi, K., 2017. "De-financialization" of commodities? Evidence from stock, crude oil and natural gas markets. Energy Econ. 68, 228–239. http://dx.doi.org/10.1016/j.eneco.2017.09.024.

Zhang, D., Ji, Q., 2018. Further evidence on the debate of oil-gas price decoupling: A long memory approach. Energy Policy 113, 68–75. http://dx.doi.org/10.1016/j.enpol.2017.10.046.

Zhong, M., Darrat, A.F., Otero, R., 2004. Price discovery and volatility spillovers in index futures markets: Some evidence from Mexico. J. Bank. Financ. 28 (12), 3037–3054. http://dx.doi.org/10.1016/j.jbankfin.2004.05.001.